Technical Medicine Master of Science Thesis

Determination of stent patency and flare geometry of balloon expandable covered stent grafts in patients after fenestrated endovascular aortic aneurysm repair

Claire van der Riet

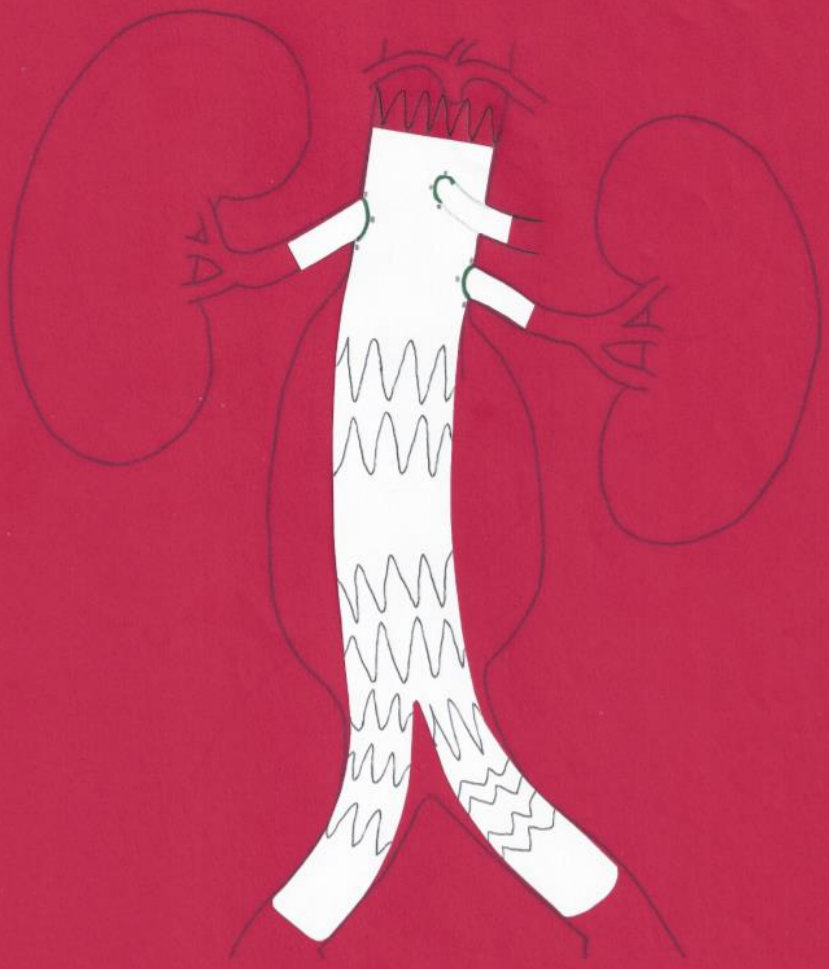

UNIVERSITY OF TWENTE.

June 2020

umcg

Determination of stent patency and flare geometry of balloon expandable covered stent grafts in patients after fenestrated endovascular aortic aneurysm repair

Author: Claire van der Riet
Student number: s1490826
Date: May 28th, 2020

Technical Medicine, track Medical Imaging and Interventions
University of Twente
Enschede, The Netherlands

Department of Vascular Surgery
University Medical Center Groningen
Groningen, The Netherlands

UNIVERSITY OF TWENTE.

umcg

Graduation committee

Chairman and Technical Supervisor	Prof. dr. ir. C.H. Slump *University of Twente, Enschede, The Netherlands*
Clinical Supervisor	Prof. dr. J.P.P.M. de Vries *UMC Groningen, The Netherlands*
Technical Medicine Supervisor	Dr. R.C.L. Schuurmann *UMC Groningen, The Netherlands*
Process Supervisor	R.J. Haarman, MSc. *University of Twente, Enschede, The Netherlands*
External Member	Dr. E.J.F.M. ten Berge *University of Twente, Enschede, The Netherlands*

Extra supervisors

Dr. I.F.J. Tielliu
UMC Groningen, The Netherlands

Dr. R.P.H. Bokkers
UMC Groningen, The Netherlands

Preface

Seven years as a student of Technical Medicine is coming to an end with this master thesis. In it I hope to show the results of the steps I have made in my development from a first-year student to the technical physician that I am about to become.

In the past 10 months, I completed my graduation internship at the vascular surgery department of the UMC Groningen. For me, a different hospital and new colleagues in an unknown city. It was an inspiring experience and I enjoyed every part of it; working hard, developing myself in clinical activities and completing two different research parts. Now I can present my Master's thesis, but not before thanking a number of people for their support.

First of all, I would like to thank my supervisors of UMC Groningen, Jean-Paul de Vries and Richte Schuurmann. Jean-Paul knew exactly what to focus on and gave me helpful feedback on how to commit my research work to paper. Richte Schuurmann, a technical physician himself, always helped me and had interesting ideas about the validation of the software. An Tournicourt, thank you for the lessons I have learned from you on how to make patients feel at ease and for making me feel more confident when performing polyclinical work and assisting during vascular surgery procedures.

Thank you, professor Slump for being my technological supervisor during the last two years and as the chairman of my graduation committee. I appreciate the numerous critical questions you posed to me and how you made me rethink topics that I thought I had figured out. Rian Haarman, thank you for being my mentor during the past two years and for making me talk about myself and helping me in making the right decisions. Thank you, Erik ten Berge for all animated interactive clinical lessons at the university of Twente and being the external member of my graduation committee.

Kirsten, Marjolein, Simone, Philippe and Friso, I enjoyed your company during shared coffee breaks and lunches. You provided exactly the kind of level-headedness that I needed. Thanks to all of you, for making me feel comfortable and, helping me with many other things and for welcoming me to come and join you as a PhD candidate after my graduation.

Lastly, it goes without saying that I am very happy with the unwavering support in every possible way from my parents, my brother and Lars, during these past years.

List of abbreviations

3D: three-dimensional
AAA: abdominal aortic aneurysm
ASA classification: American Society of Anesthesiologists classification
BECS: balloon expandable covered stent graft
CE: “Conformité Européene”
CLL: center lumen line
COPD: chronic obstructive pulmonary disease
CT: computed tomography
CTA: computed tomography angiography
DUS: duplex ultrasonography
ECG: electrocardiogram
eGFR: estimated glomerular filtration rate
EVAR: endovascular aneurysm repair
FEVAR: fenestrated endovascular aneurysm repair
FSG: fenestrated stent graft
FU: follow-up
ICU: intensive care unit
IQR: interquartile range
kV: kilovoltage
LRA: left renal artery
mAs: milliampere-seconds
mm: millimeter
MRA: magnetic resonance angiography
PTFE: polytetrafluoroethylene
RC: repeatability coefficient
RRA: right renal artery
SD: standard deviation
SMA: superior mesenteric artery
US: ultrasonography

Contents

Chapter 1 - General introduction

Clinical background

A standard diameter of an abdominal aorta is less than 20 mm in adults. An AAA is defined as an aorta with a diameter that exceeds 30 mm or is 1.5 times larger than the original diameter[1]. An aneurysm is defined as the permanent localized bulging of an artery, caused by pathological weakening of the structural integrity of the vessel wall[2]. Overtime, repeated blood pressure due to the cardiac cycle on the weakened aortic wall can cause enlargement of the aneurysm. The risk of rupture increases with aneurysm size.

Diagnosis

The incidence of an AAA ranges between 4.1% and 14.2% in men, and 0.4% and 6.2% in women, respectively[3]. Well defined risk factors of developing an AAA include advanced age, male gender, a positive family history, smoking, obesity, and atherosclerosis[4]. Rupture of the aneurysm is associated with a mortality rate of 65 – 85%[5]. Therefore, elective intervention is advised when the risk of death from aneurysm rupture exceeds the risk of the surgical procedure. An AAA diameter of 55 mm for men and 52 mm for women, or annual growth of 10 mm are indicators for an elective intervention[6].

An AAA is diagnosed by imaging techniques such as CT, MRA, US and/or X-ray. A CTA is performed to localize the aneurysm relative to the visceral arteries. An AAA is named after the location in a specific segment of the abdominal aorta. Suprarenal AAA is defined as an aneurysm that involves the visceral arteries (Figure 1). Pararenal AAA is defined as an aneurysm that involves the renal arteries but not the mesenteric arteries. Juxtarenal AAA is defined as an aneurysm that extends up to but does not involve the renal arteries and infrarenal AAA is located distal to the renal arteries[7].

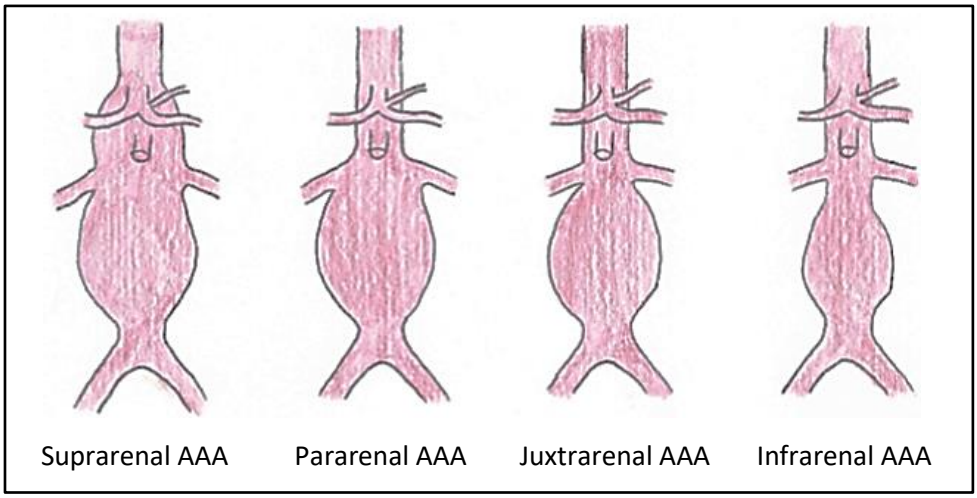

Figure 1: Classification of AAA relative to the renal arteries: suprarenal, pararenal, juxtarenal and infrarenal. Figure adapted from Febbo et al.[8]

Treatment

Two types of surgical intervention to treat an AAA are currently available: open repair and EVAR. EVAR is a minimally invasive procedure with shorter recovery time and reduced 30-days morbidity and mortality rate. Complications of both operations include cardiac and respiratory problems, ischemic colitis, renal insufficiency, lower extremity ischemia and bowel ischemia. The 30-day complications are, however, significantly lower after EVAR than after open repair[9]. Furthermore, hospital and ICU length of stay are lower after EVAR[10, 11].

In case of a complex AAA, such as a juxta-, para- or suprarenal AAA, a custom-designed endograft with a notch (scallop) and holes (fenestrations) to perfuse the visceral arteries can be used (Figure 2)[12]. This surgical procedure is called FEVAR and makes use of a stent graft with fenestrations and with or without a scallop. This stent graft is called the FSG. The LRA, the RRA, the SMA and the celiac trunk are common fenestrations. The anatomy and location of the aneurysm both dictate which visceral arteries become part of the FSG. FEVAR can be a technically challenging surgical procedure where the experience of the vascular surgeon and intervention radiologist plays a major role in connecting the fenestrations to the FSG[13].

These FSGs are customized to each patient and the manufacturing takes multiple weeks. BECSs were frequently used to stent the visceral arteries, because of the higher (short-term) patency rates than the uncovered stent[14, 15]. The BECS is covered with PTFE film technology and is designed to conform to the vessel structure. The stainless-steel struts are completely covered protecting both the flow lumen as well as the struts from contact with the endothelium of the arteries. There are different diameter and length sizes available.

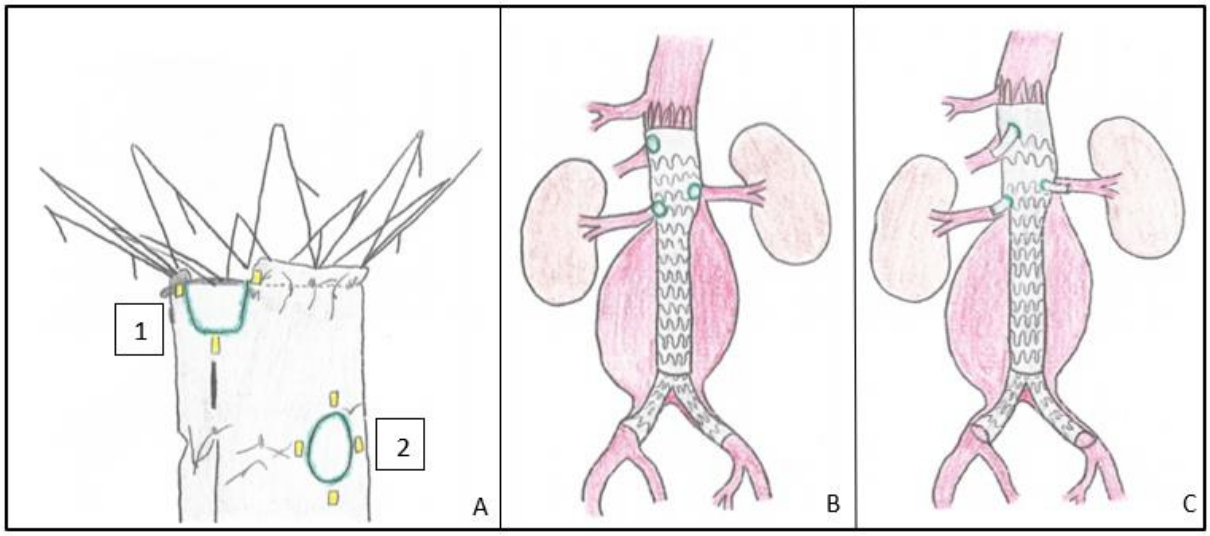

Figure 2: A) FSG with a scallop(1) and a fenestration(2), B) Illustration showing deployment of the FSG with three fenestrations, C) Illustration showing deployment of the FSG and BECS in the LRA, RRA and SMA. Figure adapted from Hu et al.[16]

Outline of this thesis

This master thesis is divided into two research parts: a clinical and a technical chapter. The clinical research in chapter 2 is about patient's outcome who were treated with FEVAR and the patency of the BECS. The technical research in chapter 3 is about the in vitro validation of a new methodology to detect subtle changes in position and patency of the BECS in the visceral arteries during patient's follow-up.

Chapter 2 - Patency of balloon expandable covered stent in patients after fenestrated endovascular aneurysm repair

The Advanta V12 (Atrium Medical Corporation, Hudson, NH, USA) BECS is CE marked for restoring and improving the patency of iliac and renal arteries. We are interested in the patency and re-intervention rates of the Advanta V12 BECS, when it is used in the fenestration of the FSG by FEVAR. BECS are secured in the fenestrations of the FSG by the flare (Figure 3). Hemodynamic forces that act on this connection, can affect the position of the FSG and the BECS in the fenestration. Suboptimal flaring or mismatch between the fenestration and the BECS during the FEVAR procedure, and changes herein during follow-up may result in BECS displacement and BECS-specific endoleaks. Changes of the BECS configuration in the fenestration such as translation and rotation during follow-up can also cause compression or kinking of the BECS which can lead to stenoses, occlusions or a fracture of the BECS[17]. Stent fractures in the renal arteries have been documented for some individual cases. Less commonly described locations of stent fracture are the SMA and the celiac trunk[18, 19]. The research question is: "What is the patency of the Advanta V12 BECS in a consecutive cohort of FEVAR patients?".

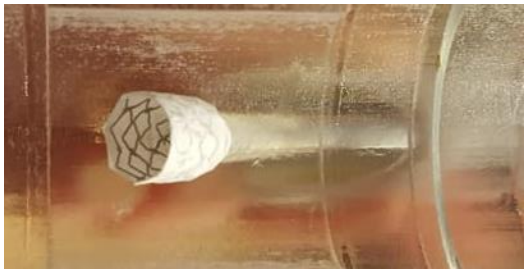

Figure 3: A flared BECS in an in vitro aorta phantom model

Chapter 3 - Quantitative flare geometry of balloon expandable stent grafts; in vitro validation

Accurate 3D assessment of the BECS geometry within the fenestration of the FSG has not been determined before but is likely to reveal essential modes of failure. It should reveal modes of failure in an early state, before urgent re-intervention is necessary. This may enable patient-tailored imaging follow-up, prevent complications, and improve treatment options during re-interventions. Knowing these modes of failure will help the vascular surgeon and the intervention radiologist to optimize treatment (i.e. sizing, planning and flaring), and manufacturers to optimize the design of the BECS.

The results of this study may aid in designing a 3D post-FEVAR measurement protocol for accurate assessment of (changes in) the configuration in a vascular workstation with reconstructed CT images. Dedicated home-made imaging software was developed to systematically and accurately assess the BECS geometry for visualization and quantification, see chapter 3. This new methodology needs to be validated; the research question is: "Can we accurately determine the flare geometry of BECSs in an in-vitro aorta model (over time) with dedicated imaging software?".

Chapter 4 – Future perspectives

Overview of the amendments to the software and additional research which is needed to facilitate clinical implementation is given. Suggestions to optimize stent design and the FEVAR procedure were mentioned.

Chapter 2 – Patency of balloon expandable covered stent in patients after fenestrated endovascular aneurysm repair

Abstract

Objective: FEVAR is used for treatment of a complex AAA in which visceral arteries are incorporated. Re-interventions and BECS related complications have been reported frequently after FEVAR. Clinical outcomes and patency rates of Advanta V12 BECS used as bridging stents in FEVAR are presented in this study.

Methods: All patients treated with FEVAR or suprarenal fenestrated re-intervention of previous EVAR with at least one fenestration treated with an Advanta V12 BECS in UMC Groningen, The Netherlands or Klinikum Süd, Germany between January 2012 and December 2015 were included. Primary end points were technical success, re-intervention rates and mortality. Secondary end points were BECS patency, defined as the absence of stenosis, occlusion, type 3 endoleak and a stent fracture, at last follow-up surveillance.

Results: A total of 195 FEVAR patients with a mean age of 72.2±8.0 years met the inclusion criteria. Advanta V12 BECS were placed in 458 target arteries (174x LRA, 179x RRA, 91x SMA, 14x celiac trunk). Median follow-up time based on the latest CTA and DUS surveillance was 29.3±26.5 months. Technical success was obtained in 181 patients (93%). 34 patients died during FU, 14 of them were AAA-related and six of them were in-hospital mortality. In total, 43 re-interventions were performed, the freedom from re-intervention is 61% at 4 years. 27 Advanta V12 BECS (6%) suffered a complication during follow-up; four BECSs had a stenosis, six BECSs had an occlusion, eleven BECS had a type 3 endoleak and three BECSs were fractured. In addition, one BECS had both a type 3 endoleak and a stenosis, one BECS was fractured and had a stenosis, and one BECS was fractured and had an occlusion. 16 re-interventions were performed for 18 complicated Advanta V12 BECS.

Conclusion: 13% of FEVAR-patients underwent a re-intervention at 1 year and 39% at 4 years. Advanta V12 BECSs used as bridging stents showed favorable outcomes. Patency rates were 93% at 1 year and 88% at 4 years. Early detection of complications is needed to prevent urgent re-intervention. FSG migration and diameter measurement of the target arteries pre- and post-FEVAR will provide more information about the changes in BECS configuration over time.

Introduction

FEVAR is associated with high technical success (99%), low perioperative mortality (4.1%) in comparison to open repair, and low intraoperative target artery occlusion (0.6%)[20]. Within three to five years after the primary procedure, re-interventions are, however, reported in 11% to 44% of FEVAR patients, which are related to stenosis or occlusion of target arteries in 5% to 15% and to BECS-associated endoleaks in 4% to 10%[20-22]. Potential causes for these complications are mismatch in diameter between the fenestration and the BECS, suboptimal flaring of the BECS during the FEVAR procedure and material failures. Post-operative imaging surveillance is important to detect complications on time, before urgent re-intervention of BECS obstruction or endoleak is required[23].

In the follow-up after a FEVAR, CTA and DUS are frequently used imaging modalities[24, 25]. Current guidelines recommend post-FEVAR CTA follow-up at several time intervals (Figure 4). CTA detects most FSG and BECS complications such as stenosis, occlusion, endoleaks and stent fractures. Disadvantages of CTA are the amount of exposure to ionizing radiation, when frequently repeated imaging is required, and the use of nephrotoxic contrast in patients with pre-existing renal dysfunction. DUS is a low-cost imaging technique that detects and visualizes endoleak flow direction, without exposing the patient to ionizing radiation or nephrotoxic contrast. Nevertheless, substantial inter-observer variability is a limitation of DUS in measuring the diameter of the aneurysm and DUS lacks information about FSG and BECS migration and stent fractures.

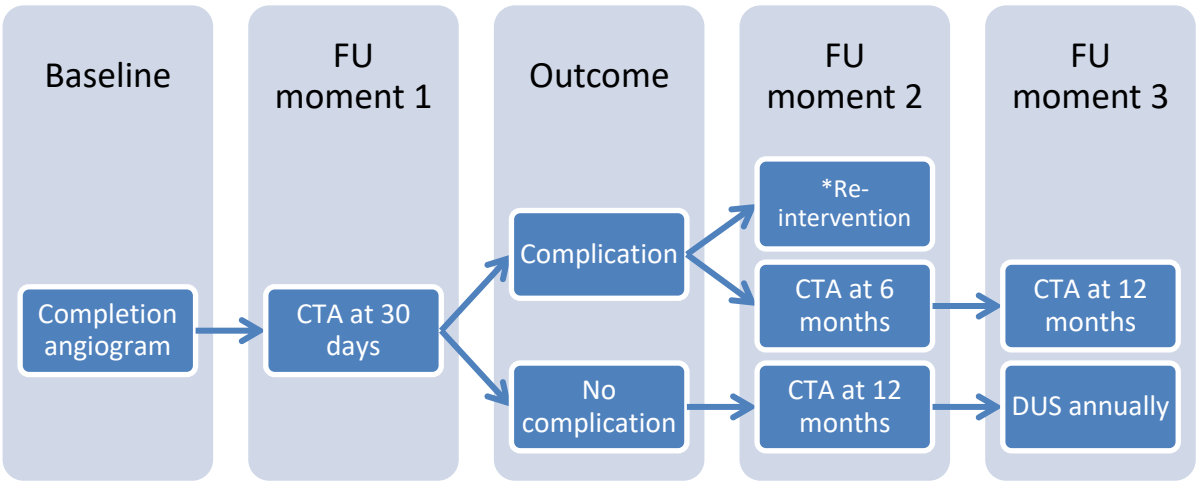

*Figure 4: FEVAR follow-up flow chart, *return to follow-up moment 1 in case of a re-intervention*

Endoleaks are characterized by persistent blood flow within the aneurysm sac post-FEVAR (Figure 5). There are five different types of endoleak as shown in Table 1. Type 1 endoleaks arise at the ends of the endograft due to inadequate seal between the graft material and the inner wall of the artery. This type of endoleak can occur at the proximal or distal end, defined as type 1a and type 1b endoleak, respectively. Type 1c is defined as an endoleak at the distal end of the BECS. Type 2 endoleaks describe retrograde filling of the aneurysm sac via a visceral artery.

Type 3 endoleaks are caused by a defect in the endograft due to mechanical failure or junctional separation of the modular components; type 3a is related to aortic components, type 3b is related to iliac limb components and type 3c is related to BECSs. Causes may relate to device failures, extreme angulation of a segment predisposing to fracture or improper overlap of the modular components during the FEVAR. Type 3d describes the graft tear, a perforation, or a fracture of the BECS.

Type 4 endoleaks describe a locally porous graft. Endotension defines a continued expansion of the aneurysm sac without radiographic evidence of an endoleak. High-pressure endoleaks, such as type 1

and type 3 endoleaks, require urgent re-intervention because of the relatively high risk of a rupture. Low-pressure endoleaks, such as type 2 and endotension are considered less urgent to repair but need continued CTA surveillance and a re-intervention if there is ongoing growth of the aneurysm sac[26, 27].

In this retrospective study, the patency of Advanta V12 BECS used as bridging stents in patients who were treated by FEVAR for a suprarenal, pararenal or juxtarenal AAA were evaluated.

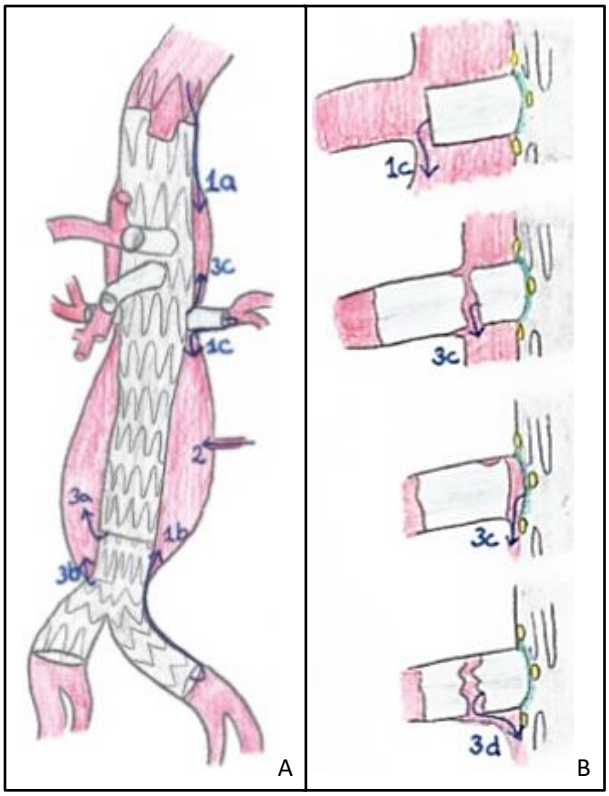

Figure 5: A) FEVAR-related endoleaks, B) BECS-associated endoleaks. Figure adapted from Jain et al.[28]

Table 1: Categorization of different types of endoleak

Endoleak	Definition
Type 1	Inadequate seal of FSG a) Proximal end b) Distal end c) BECS end
Type 2	Retrograde filling of the aneurysm sac by inferior mesenteric artery and/or lumbar arteries
Type 3	Defect in the endograft a) Aortic-aortic or aortic-bifurcated component b) Bifurcated-iliac limb or iliac limb-iliac limb component c) FSG-BECS or BECS-BECS component d) Graft tear, perforation or fracture
Type 4	Porous endograft
Endotension	Aneurysm sac enlargement without visualized endoleak

FSG: fenestrated stent graft
BECS: balloon expandable covered stent

Methods

Patients and BECSs inclusion

Patients with an AAA treated by FEVAR were included from two high-volume FEVAR centers; 66 patients from University Medical Center Groningen (UMCG), The Netherlands and 142 patients from Klinikum Süd, Nuremberg, Germany. Between January 2012 and December 2015, 208 patients underwent FEVAR (Figure 6). Inclusion criteria for the study were: patients treated with initial FEVAR or suprarenal fenestrated re-intervention of previous EVAR with at least one fenestration treated with an Advanta V12 BECS. The study was approved by the institutional review boards and the study was conducted according to the Declaration of Helsinki.

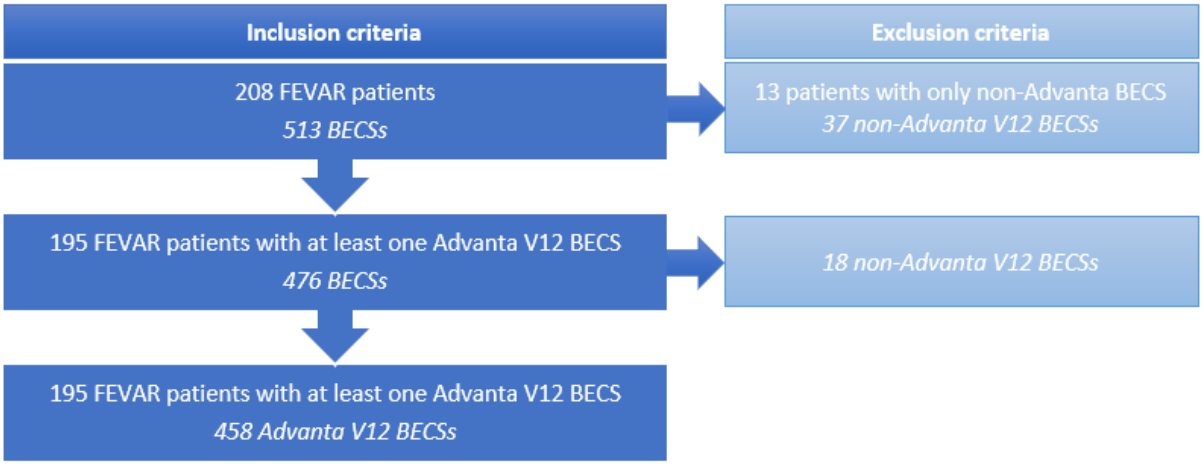

Figure 6: Flow chart of patient and BECS inclusion

Measurements

Clinical data as available until November 2019 was retrospectively collected from the electronic patient records and registered in REDCap, a web-based data capture platform for clinical research. The clinical outcome variables are:

- Patient demographics: age, gender, baseline eGFR, ASA classification, pre-operative aneurysm diameter and the presence of hypertension, diabetes mellitus, ischemic heart disease and COPD. The presence of hypertension is registered if the patient uses one or more antihypertensive drugs.
- Procedural characteristics: FEVAR procedure date, additional unplanned procedures, presence of endoleak on completion angiogram, procedure time, FEVAR-related complications and technical success. Technical success is defined as successful deployment of the FSG and BECS(s) without visible type 1 or 3 endoleak at the completion angiography.
- FSG and BECSs characteristics: type and size of FSG, number of scallops and fenestrations and the size of Advanta V12 BECSs.
- Early outcomes: length of ICU and hospital stay, in-hospital mortality, complications, re-admissions and aneurysm-related re-interventions. Complications are defined as stenosis, occlusion, occurrence of different types of endoleak, and stent fractures.
- Follow-up outcomes: date and complications on post-FEVAR CTA and DUS surveillance per patient and per BECS, duration of follow-up per imaging modality, date and indication of AAA-related re-interventions and all-cause and AAA related mortality.

Statistical analysis

Data were analyzed using SPSS version 23 statistical software (SPSS Inc., Chicago, Ill). Normality of the data was assessed via visual inspection of Q-Q plots. All variables showed a normal distribution, so the

data are expressed as mean±SD. Kaplan-Meier curves were constructed to estimate the survival curve and re-intervention free survival of patients. Furthermore, survival curves were performed for re-intervention and complication-free survival of all BECSs. Complication-free survival is visualized for all BECSs as a total and per fenestration.

Results

In total, 195 patients (mean age 72.3±8.0 years; 84% male) who met the inclusion criteria were included of which 188 were treated with a Zenith FSG (Cook Medical Inc., Bloomington, IN, USA) and seven patients were treated with an Anaconda FSG (Terumo Aortic, Inchinnan, Scotland, UK). Seventeen patients were treated with a fenestrated cuff for the treatment of a type 1a endoleak to solve a failed standard EVAR. Patient demographics are shown in Table 2.

The FSG and target arteries characteristics are shown in Table 3. In total, there were 153 scallops and 458 fenestrations were stented with an Advanta V12 BECS. Sixteen patients had an Advanta V12 BECS and a non-Advanta V12 BECS in situ for different fenestrations but only the Advanta V12 BECSs were included for the BECS analysis.

Table 2: Demographics of fenestrated endovascular aortic repair patients

Variable	Total (N=195)
Age (years)	72.2±8.0
Gender:	
• Male	163 (84%)
• Female	32 (16%)
eGFR (mL/min)	61.0±20
Hypertension	161 (83%)
Diabetes mellitus	27 (14%)
Ischaemic heart disease	105 (54%)
COPD	80 (41%)
Pre-FEVAR aneurysm diameter (mm)	59.7±10.2
ASA classification:	
• 2	99 (51%)
• 3	88 (45%)
• 4	7 (4%)
• Not specified	1 (1%)

eGFR: estimated glomerular filtration rate
COPD: chronic obstructive pulmonary disease
FEVAR: fenestrated endovascular aneurysm repair
ASA classification: American Society of Anesthesiologists classification

Table 3: Fenestrated stent graft and target artery characteristics

Endograft	Total
Type of FSG	*(N=195)*
• Zenith	188
• Anaconda	7
Number of total fenestrations	*(N=195)*
• 1	16
• 2	92
• 3	72
• 4	15
BECS	*(N=458)*
• Celiac trunk	14
• SMA	91
• RRA	179
• LRA	174

FSG: fenestrated stent graft
BECS: balloon expandable covered stent
SMA: superior mesenteric artery
RRA: right renal artery
LRA: left renal artery

Early clinical outcomes

Technical success was obtained in 181 out of 195 patients (93%); 6 patients had an endoleak (4x type 1a endoleak, 1x type 3 endoleak of the LRA), in 3 patients a renal artery (1x LRA and 2x RRA) was lost due to a dissection, in 1 patient the RRA was lost due to stenting a lumbar artery instead of the RRA, 1 patient had an occluded LRA, the internal iliac artery was covered (not intended) in 1 patient and in 2 patients the FEVAR procedure was not completed.

The FEVAR procedure was not completed due to the following reasons; 1x the RRA could not be cannulated and stented, this patient underwent a re-intervention to stent the RRA, and 1x the celiac trunk was not connected because of the duration of the procedure and the large amount of contrast that was used. This patient fell out of bed twice and died due to a subdural hematoma with evident midline shift at day 3 post-FEVAR.

The early post-operative FEVAR procedure results are shown in Table 4. Three patients stayed longer than 6 days at the ICU. One patient stayed for 10 days due to renal insufficiency (lumbar artery stented instead of RRA, mentioned above) and a hospital acquired pneumonia, one patient stayed for 15 days due to renal insufficiency (LRA dissection, mentioned above) and another patient stayed for 62 days at the ICU and died in-hospital due to multiorgan failure. In total, six patients (3%) died during hospitalization due to the following reasons: 3x multiorgan failure (one is already mentioned), 2x bowel ischemia, 1x the patient fell out of bed twice (mentioned above).

All re-interventions within 30 days after the FEVAR procedure were performed during hospitalization of the FEVAR procedure. One patient (1%) was readmitted to the hospital within 30 days due to a fever, this was classified as post implantation syndrome. This is the clinical and biochemical expression of an inflammatory response following FEVAR.

Table 4: Early post-FEVAR outcomes

Variable	Total (N=195)
Length of hospital stay (days)	6.3±4.7
Length of ICU stay (days)	0.9±4.8
In-hospital mortality	6 (3%)
30-days readmission	1 (1%)
30-days re-intervention	7 (4%)

ICU: intensive care unit

Follow-up clinical outcomes

The mean of the last CTA follow-up time was 23.9±23.9 months in Klinikum Süd and 35.7±30.3 months in UMCG. The mean last follow-up time (based on CTA and DUS surveillance) for both hospitals was 29.3±26.5 months. Table 5 shows all indications for the first re-intervention per patient.

Table 5: Indication for first re-interventions

Variable	Patients (N=43)
Rupture due to:	
Type 1b endoleak	1
Type 2 endoleak	1
Type 3c endoleak	1
Endoleak:	
Type 1a	*3
Type 1b	1
Type 1b and 3b	1
Type 1b and 1x type 3c (LRA)	1
Type 1b and 3x type 3c (LRA, RRA, SMA)	1
Type 1c (LRA)	1
Type 2	9
Type 2 and type 3c (LRA)	1
Type 3c (2x LRA, 2x RRA, 1x celiac trunk)	*5
Stenosis and occlusion in BECS:	
Stenosis of LRA	1
Stenosis and stent fracture of RRA	1
Occlusion of LRA	1
Occlusion of LRA and stenosis of RRA	1
Complications iliac trajectory:	
Stent fracture	2
Dislocation	1
Dissection of external iliac artery	*1
Bleeding:	
External iliac artery in the groin	**2
Left kidney	**2
Complications of visceral arteries in a scallop (1x SMA, 1x celiac trunk)	2
FEVAR procedure not completed	1
Growing aneurysm sac	1
FSG infection	1

** one 30-days re-intervention*
LRA: left renal artery
RRA: right renal artery
SMA: superior mesenteric artery
BECS: balloon expandable covered stent
FEVAR: fenestrated endovascular aneurysm repair
FSG: fenestrated stent graft

The freedom from re-intervention is visualized in a Kaplan-Meier curve (Figure 7). Eight patients out of 43 patients who have had a re-intervention underwent multiple re-interventions (Figure 8). In total, 34 patients died during follow-up, 14 of them were AAA-related. The overall survival is visualized in a Kaplan-Meier curve (Figure 9).

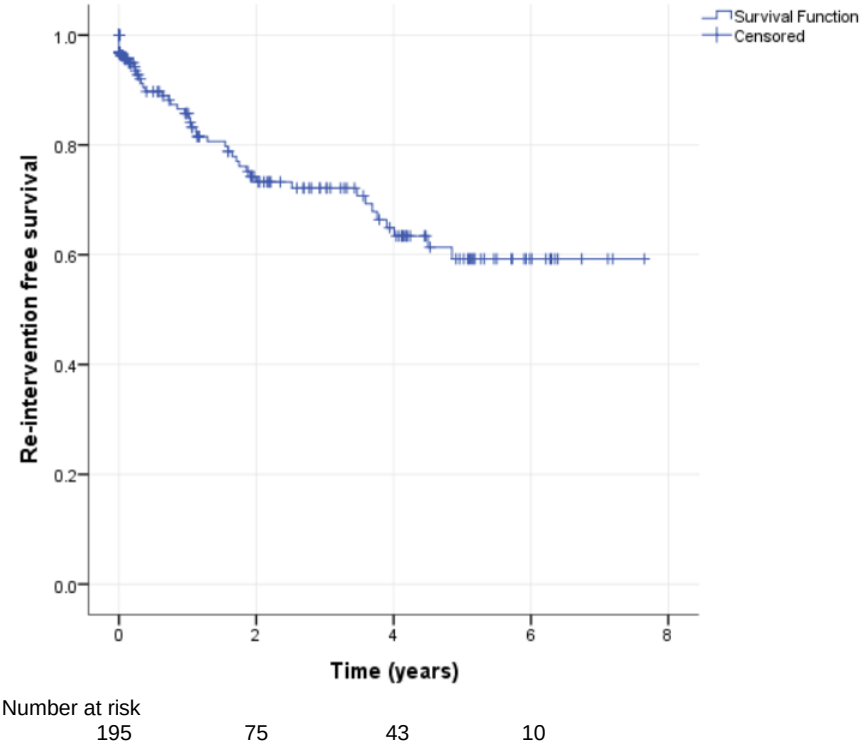

Figure 7: Kaplan-Meier curve for re-intervention free survival of FEVAR-patients

Re-intervention	1	2	3
Patient 1	Day 139: Type 3c endoleak of celiac trunk	Day 156: Stent fracture of SMA	Day 2559: Occlusion of RRA
Patient 2	Day 266: Stenosis of LRA	Day 1041: Type 3c endoleak of SMA	
Patient 3	Day 371: Type 3c endoleak of LRA	Day 406: Type 3c endoleak of LRA	
Patient 4	Day 602: Stenosis and stent fracture of RRA	Day 2218: Embolisation of internal iliac artery	
Patient 5	Day 624: Type 1b endoleak	Day 776: Renal bleeding	
Patient 6	Day 638: Endoleaks: type 1b and 3x type 3c	Day 1458: Stenosis left iliac limb	Day 1463: Claudication and kink of left iliac limb
Patient 7	Day 918: Rupture (type 2 endoleak)	Day 965: Rupture	
Patient 8	Day 1035: Endoleaks: type 1b and type 3b	Day 1167: Type 3b endoleak	

Figure 8: Overview of patients and their indications for multiple re-interventions

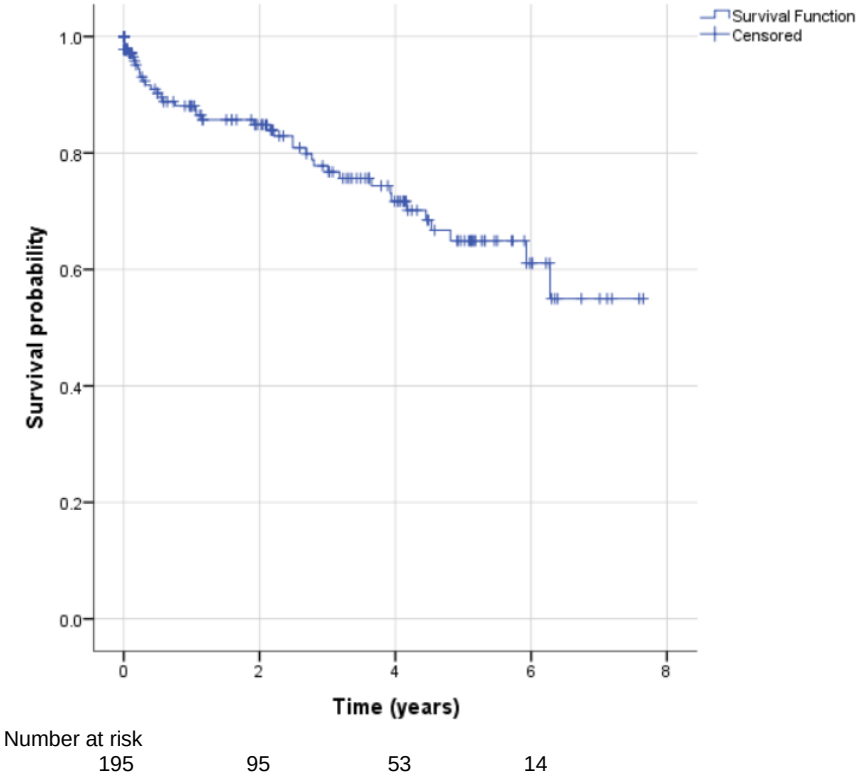

Figure 9: Kaplan-Meier survival curve for FEVAR patients with Advanta V12 BECS(s)

Advanta V12 BECS outcomes

431 out of 458 Advanta V12 BECS had an uncomplicated follow-up. 27 (6%) Advanta V12's suffered a complication; four BECSs (0.9%) had a stenosis, six BECSs (1.3%) had an occlusion, eleven BECS (2.4%) had a type 3 endoleak and three BECSs (0.6%) were fractured. In addition, one BECS (0.2%) had both a type 3 endoleak and a stenosis, one BECS (0.2%) was fractured and had a stenosis, and one BECS (0.2%) was fractured and had an occlusion (Figure 10). 16 re-interventions were performed for 18 Advanta V12 BECS related complications.

The freedom from complications of all BECS and per fenestration were presented as a Kaplan-Meier curve (Figure 11 and 12). BECSs that had not required a re-intervention were presented as a re-intervention free survival curve (Figure 13).

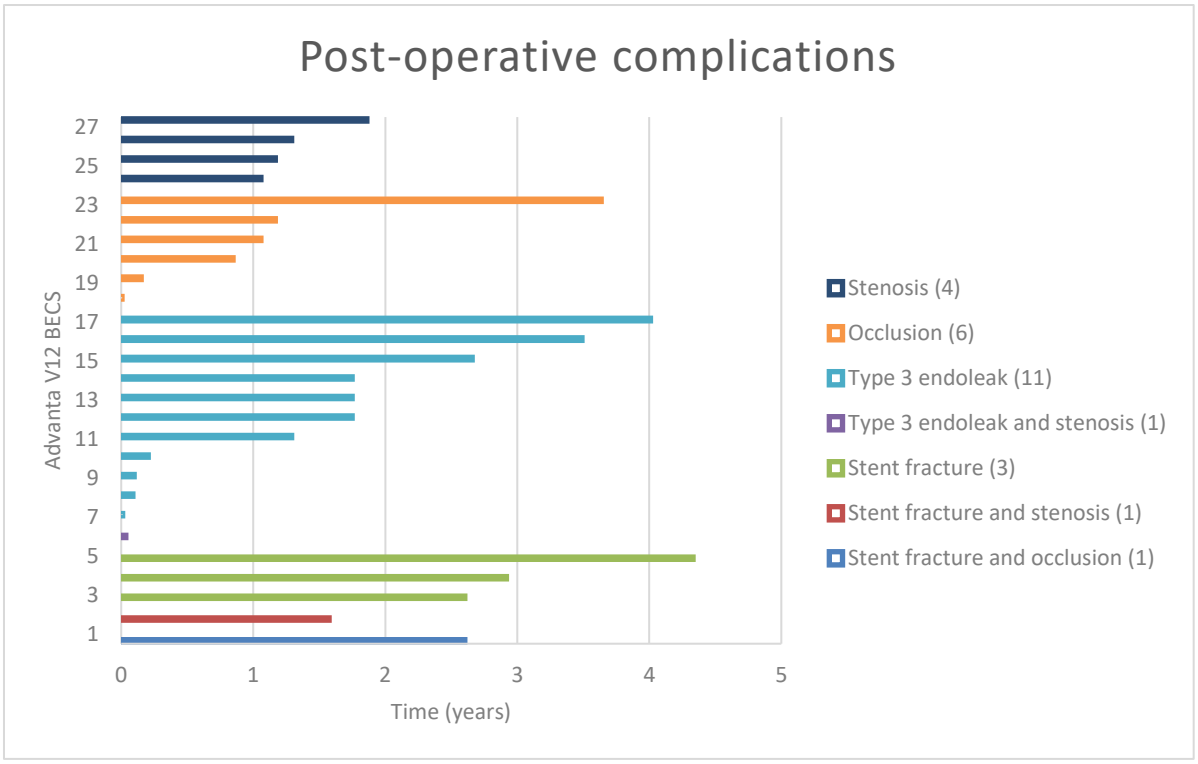

Figure 10: Occurrence of post-operative BECS complications over time in years

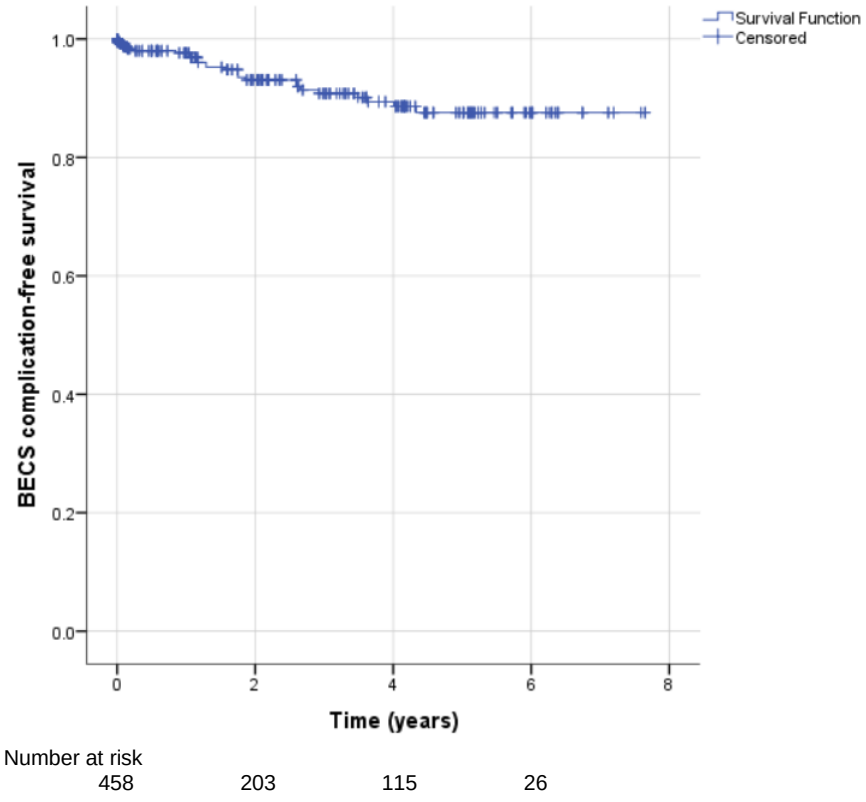

Figure 11: Kaplan-Meier curve for Advanta V12 BECS complication-free survival

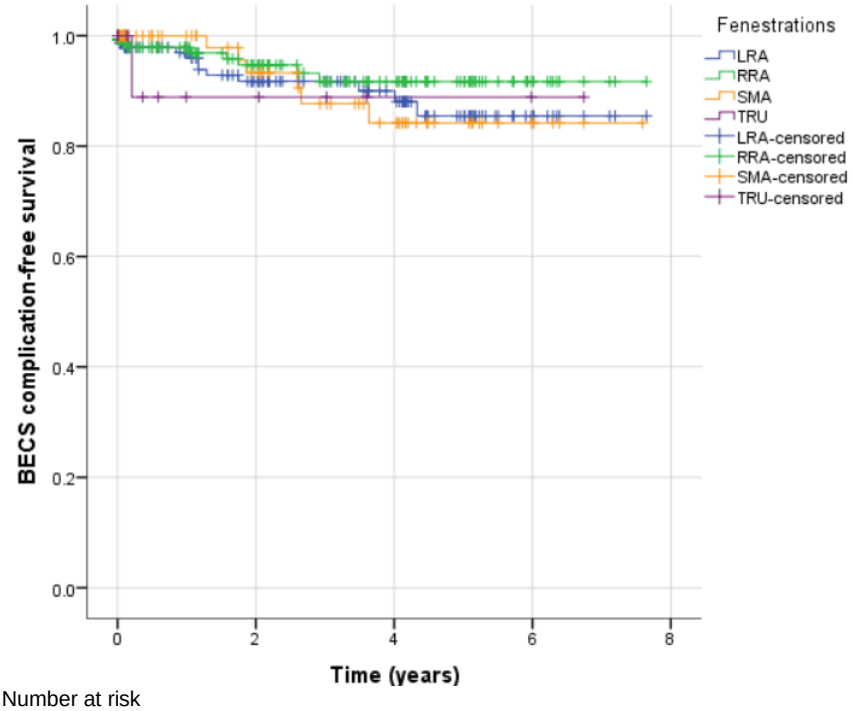

Number at risk

LRA	174	78	46	10
RRA	179	80	44	10
SMA	91	40	23	5
TRU	14	5	2	1

Figure 12: Kaplan-Meier curve for Advanta V12 BECS complication-free survival visualized per fenestration

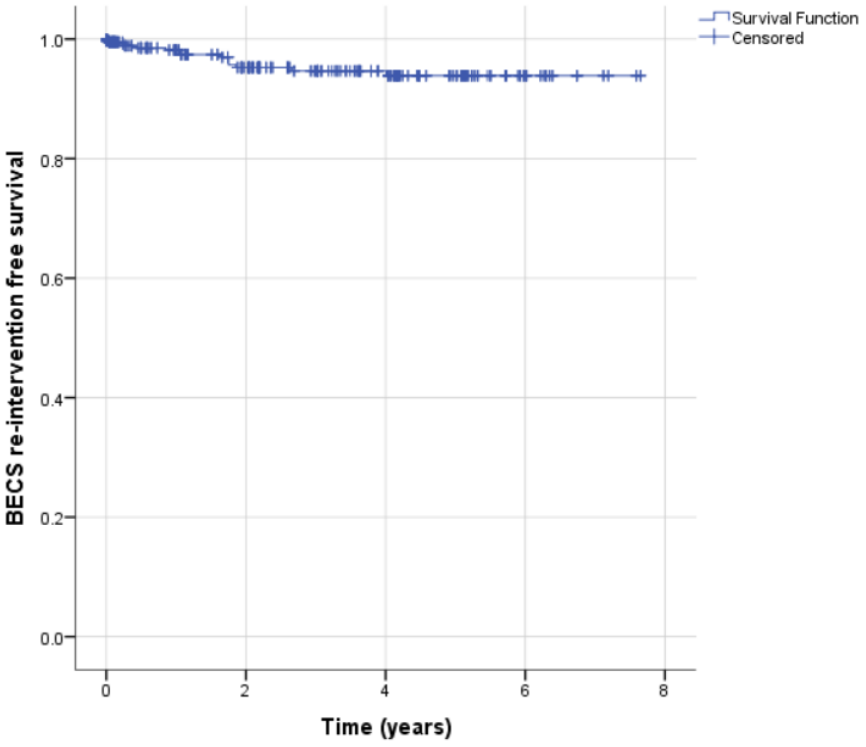

Number at risk

458	210	120	28

Figure 13: Kaplan-Meier curve for re-intervention free survival of Advanta V12 BECS

Discussion

The purpose of this study was to investigate the Advanta V12 BECS patency in FEVAR patients. We have focused on re-interventions, patient's survival and complications per patient and per BECS. The number of complications, the survival curve and the AAA-related deaths may be underestimated because these reflect only the patients who went to the hospital. The complications such as stenosis, occlusion, type 3 endoleak and stent fracture are registered according to the radiological report or performed re-interventions.

The results are based on 458 BECSs: 174 in the LRA, 179 in the RRA, 91 in the SMA and 14 in the celiac trunk. BECSs outcomes may not be generalizable to all fenestrations because more cranial located target arteries such as the SMA and the celiac trunk are significantly less stented with BECS than the LRA and the RRA. In addition, the branch arteries have their own anatomical characteristics such as the diameter and the angle at which they branch off.

Freedom from re-intervention was 61% of 195 FEVAR patients at 4 years. 43 patients underwent a re-intervention whereas 16 re-interventions for 18 BECS complications, as shown in Table 5. Two patients underwent multiple re-interventions for different fenestrations (Figure 8). Freedom from complications and freedom from re-intervention per BECS was respectively 88% and 94% at 5 years (Figure 11 and 13). Note, that not all complications needed a re-intervention.

A miscalculation in the preprocedural planning of the fenestrations and sizing of the BECS can be a mode of failure, this was not included in this study. Furthermore, migration of the FSG can affect the position of the BECS in the fenestration. At this moment, the cause of the complications of the BECS has not been revealed. Mastracci et al. underlined the importance of frequently post-operative imaging surveillance to detect changes in time[23]. FEVAR patients who were lost to follow-up could have complications and go undetected, especially in Klinikum Süd where the follow-up time was shorter than in UMCG. This results in an underestimation of the BECS complications in this study.

Even during post-operative imaging surveillance, stent fractures without complications such as an occlusion or an endoleak are difficult to detect. Therefore, the amount of stent fractures may be underestimated. There are several potential causes of a stent fracture. Firstly, caudal migration of the FSG is seen in 33% of the patients at 4 years, this migration can compress the BECS between the fenestration and the target artery[29]. Secondly, the cardiac and respiratory cycles create movement of the FSG and target arteries. BECSs implanted in the LRA may be more susceptible to fracture than those placed in the RRA, because the LRA shows more movement than the RRA due to the cranial location[30, 31]. In this study, BECSs in the LRA showed more complications than BECSs in the RRA (Figure 12). Thirdly, a mismatch between the BECS and the anatomy of the target artery may cause loss of fixation. BECSs will be subjected to extra movement and this makes them vulnerable to fracture[15]. This study reported five fractured BECSs (one had a stenosis and one had an occlusion as well). Classification of these stent fractures in combination with FSG migration and pre- and post-FEVAR diameter measurements of the target arteries will provide more information about the cause of a stent fracture and the (standard) changes over time.

Conclusion

A substantial number of FEVAR-patients underwent a re-intervention. Advanta V12 BECSs used as bridging stents showed favorable patency rates during patient's follow-up. Detection of complications before urgent re-intervention is needed to prevent urgent re-intervention. FSG migration and diameter measurement of the target arteries pre- and post-FEVAR will provide more information about the (standard) changes in BECS configuration over time.

Chapter 3 - Quantitative flare geometry of balloon expandable stent grafts; in vitro validation

Abstract

Objective: The 3D geometry of the BECS is not regularly assessed during standard post-FEVAR CTA assessment. Subtle changes in the geometry may precede migration of the BECS, endoleaks and BECS stenosis or occlusion. A standardized and validated post-FEVAR measurement protocol to identify changes in geometry of BECS is needed for early detection of complications.

Methods: In vitro validation was performed on a CTA scan of a phantom model of the aorta with three BECS in situ. Manual measurements of the BECSs in the phantom model were performed by two observers. Vascular workstation measurements derived on reconstructed CT images consist of centerline reconstructions and placement of coordinate markers. Four coordinate markers were placed at the top of the flare, four at the fenestration and four at the distal end of the BECS by two observers. Geometric analysis was reconstructed on these coordinate markers. The *flare-to-fenestration distance* was calculated from the top of the flare circumference to the fenestration. The amount of flaring was assessed with the *flare-to-fenestration diameter ratio* and BECS compression with the diameter ratio (*D-ratio*). Inter- and intra-observer variability were visualized by Bland-Altman plots and assessed by the RC.

Results: The inter-observer variability for the manual distance and diameter measurements was not significant, the mean was ±0.43 mm and ±0.10 mm, and the limits of agreement were [-0.98, 1.84] mm and [-0.37, 0.57] mm, respectively. The mean and limits of agreement for the inter-observer variability for distance and diameter measurements in mm were ±1.18 and [-0.81, 3.16], ±0.12 [-1.97, 1.73], respectively. The mean and limits of agreement for the intra-observer variability for distance and diameter measurements in mm were ±0.13 and [-1.31, 1.58], ±0.10 [-0.88, 1.08], respectively. The mean and limits of agreement for the gold standard compared to the geometric analysis of one observer for distance and diameter measurements in mm were ±0.16 and [-2.66, 2.34], ±1.12 [-0.52, 2.75], respectively. There was a significant difference for the distance measurements of the inter-observer variability of the geometric analysis and the diameter measurements of the gold standard compared to the geometric analysis. The gold standard compared to the geometric analysis showed in all BECS larger *flare-to-fenestration diameter ratio* and matching *D-ratios*.

Conclusion: The geometric analysis functions with an acceptable inter- and intra-observer variability with the current limitations, but more measurements must be performed. The accuracy of the geometric analysis is limited by the slice thickness and the centerline in the vascular workstation. The visualization can support the clinical practice, but a precise quantification is not reachable with the currently available techniques.

Introduction

FEVAR is based on a FSG with fenestrations in order to eliminate a suprarenal, pararenal or juxtarenal AAA. BECS connect the fenestration within the FSG to the target arterie and is secured by flaring the proximal stent in the fenestration with a larger sized balloon. Subtle changes in the geometry of the flare during follow-up after FEVAR may precede migration of the BECS, endoleaks and BECS stenosis or occlusion. The 3D geometry of the BECS is not regularly assessed during standard post-operative CTA assessment and current vascular workstations are not able to perform a geometric analysis of the BECS. Therefore, subtle changes in BECS displacement or BECS compression may remain undetected[32]. Dedicated imaging software has been developed to quantify and visualize the 3D flare geometry of BECS on standard post-FEVAR CTA scans[33]. This new methodology must be validated before it can be used in CTA surveillance of FEVAR patients. The goal of this study is to provide a standardized and validated post-FEVAR measurement protocol for accurate 3D assessment of (changes in) the BECS configuration.

Methods

An in-vitro phantom model of the aorta with three branching arteries is used for the validation. This validation experiment consists of four steps:

1. Experimental set up: deployment of the BECSs and CTA scan of the phantom model.
2. Manual measurements of the BECSs in the phantom model.
3. Vascular workstation measurements derived on reconstructed CT images: segmentation of the phantom, centerline reconstructions and coordinate markers were determined on the CTA reconstruction.
4. Geometric analysis: a mesh of the contrast-rich phantom lumen, centerlines and coordinate markers were loaded into the software for a geometric analysis of the BECS.

Experimental set up

The accuracy of the geometric analysis of the software is compared to manual measurements of these dimensions, which is considered the gold standard. An in vitro phantom model was created of an aorta with three branching arteries at different angles from the aorta: 45, 60 and 90 degrees. The branches printed with Solid Works version SP3 (Solid Works, Waltham, Ma) have an inner diameter of 6 mm. The phantom consists of modular detachable 3D printed transparent segments of hard plastic which are connected by perspex tubes (Figure 1).

BeGraft (Bentley InnoMed GmbH, Hechingen, Germany) BECS of 7x28 mm were deployed in each branch under fluoroscopy. The BECS were flared with a 10x20 mm Armada balloon (Abbott, Lake Bluff, Illinois, United States) by a vascular surgeon and an interventional radiologist (Figure 2). The phantom model was filled with diluted contrast fluid (Iomeron 350, dilution fraction 1:20, Bracco Imaging GmbH, Konstanz, Germany) and was anchored to the bottom of a container that was filled with water (Figure 3). The settings of the CT scanner (Somatom Force, Siemens Healthcare GmbH, Erlangen, Germany) are displayed in Table 1.

Figure 1: Detailed view of the phantom model

Figure 2: BeGraft balloon expandable covered stent flared in the 45 degrees branch of the phantom model. A) top view of the phantom model, B) look through view of the BECS, C) side view of the BECS

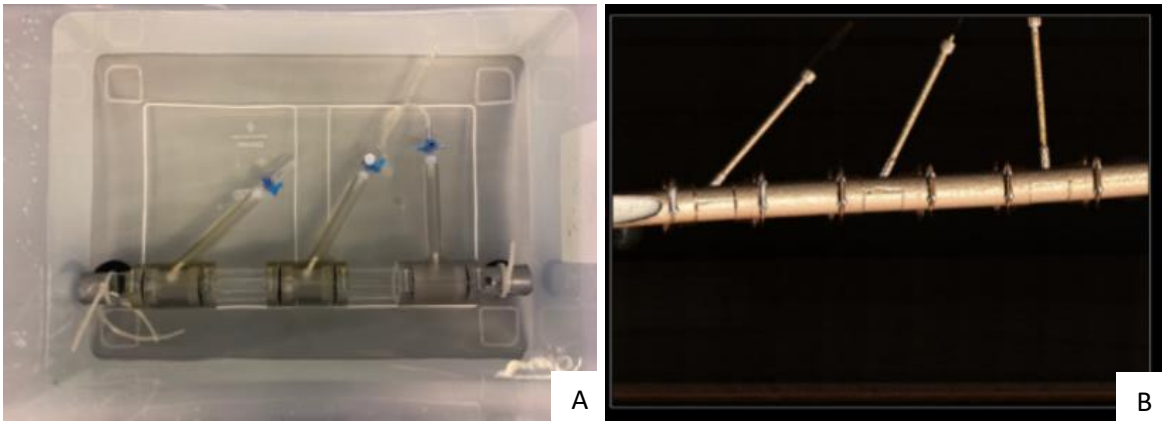

Figure 3: A) The phantom model in the container filled with water, B) 3D segmentation of the contrast-rich lumen of the phantom model

Table 1: CT settings

Variable	
Tube voltage peak	120 kVp
X-ray tube current	31 mA
Total collimation width	38.4 mm
Spiral pitch factor	0.6
Table feed	23 mm/rotation
Slice thickness	0.75 mm
Field of view	512^2
Pixel spacing	0.34\0.34 mm
Dose regulation	Admire strength 2
Reconstruction algorithm	Filtered back projection (Bv40 Force)

kVp: kilovoltage peak
mA: milliampere
mm: millimeter

Manual measurements

The manual control measurements were performed directly after the CTA scan. Four imaginary markers at the top of each flare represent the quadrants of the BECS in situ and function as reference points (Figure 4). The cranial red marker is defined as 0°, then in clockwise direction the blue marker is at 90°, the orange marker caudal is at 180° and the green marker is at 270°. Four distances and three diameters were measured by two observers (ED and CR) (Figure 5). The observers were blinded for the measurements of the other observer, in order to be able to assess inter-observer variability. The mean of the measurements of both observers function as the gold standard.

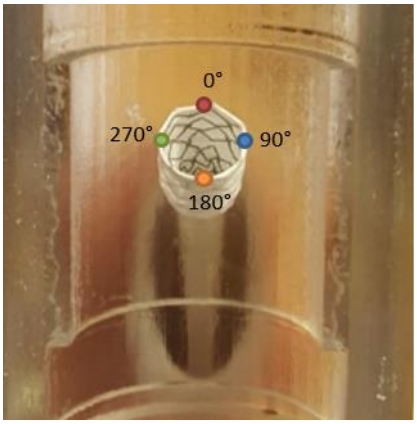

Figure 4: Different colored imaginary markers at the top of the flare

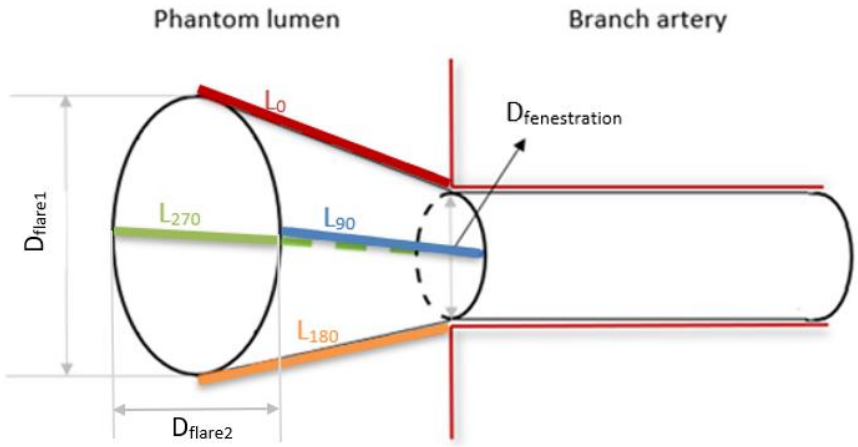

Figure 5: Schematic view of manual measurements

The distance of the flared part of the BECS to the phantom wall (*flare-to-fenestration distance*) was measured at each reference point and were named after the reference points (L_0, L_{90}, L_{180} and L_{270}). These imaginary reference points were determined by eyeballing. The distances were measured by carefully placing a caliper with a precision of 0.1 mm parallel to the BECS, careful not to displace the BECS during the measurement (Figure 6A).

The inner diameters of the BECS were measured at the top of the flare and at the level of the fenestration. At the top of the flare, two diameters were measured by a caliper, between the 0° and 180° reference points (D_{flare1}) and between 90° and 270° reference points (D_{flare2}) (Figure 6B). The minimum diameter at the level of the fenestration ($D_{fenestration}$) was carefully assessed by introducing a drill bit with increasing diameter of 0.5 mm until friction was felt (Figure 6C). A drill bit was used, because it was not possible to reach the level of the fenestration by a caliper. The D_{flare1} and D_{flare2} were measured by both observers, before the $D_{fenestration}$ was measured. This consecution of the diameter measurements is important to avoid changes in the flare by introducing a drill bit into the fenestration.

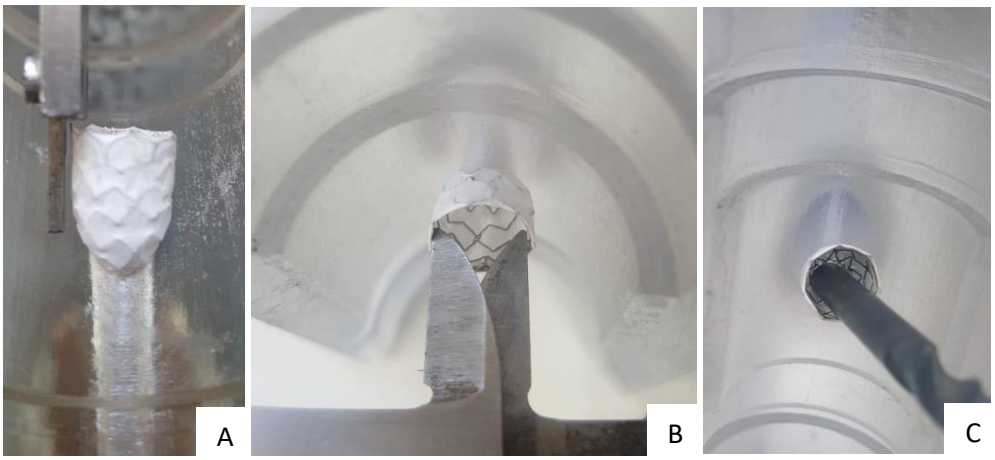

Figure 6: Examples of manual measurements: A) L_{270}, B) D_{flare}, C) $D_{fenestration}$

Vascular workstation measurements

The BECS geometry was calculated from Cartesian coordinates which were measured on a dedicated vascular workstation (3Mensio Vascular, version 10.1, Bilthoven, The Netherlands) by two observers (RS and CR). The observers were blinded from the measurements of the other observer. One observer

(CR) performed all measurements twice, in order to be able to assess inter- and intra-observer variability.

The contrast-rich lumen of the aorta phantom and its branches was segmented in 3Mensio and a center lumen line (CLL) was constructed in the main lumen and the lumina of the branch arteries. Four markers were placed in four quadrants at the top of the flare, at the fenestration, and at the distal end of the BECS (Figure 7). The 3D coordinates of the CLL's, coordinate markers and a mesh of the phantom lumen filled with diluted contrast were imported into dedicated imaging software (MATLAB, 2019b, The MathWorks Inc, Natick, Mass) for geometric analysis[33].

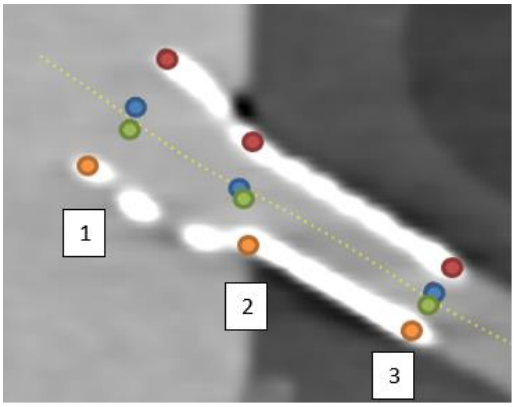

Figure 7: The BECS' CLL in yellow and the coordinate markers at the top of the flare(1), at the fenestration(2), and at the distal end of the BECS(3)

Geometric analysis

The BECS are divided into two parts: from the top of the flare to the fenestration (flared part) and from the fenestration to the distal end of the BECS (branched part) (Figure 8A). The flare geometry of the BECS is determined by three parameters:

1. *Flare-to-fenestration distance* describes the distance from the top of the flare to the phantom wall. The circumferences of the top of the flare and of the fenestration were determined by spline interpolation through the four coordinate markers. The Euclidean distance was calculated for each interpolated point on the top of the flare and its corresponding point on the fenestration (Figure 8B). The same distance calculation was performed from the distal end of the BECS to the fenestration. The sum of both distances was calculated and visualized to verify how the total length corresponds with the length of the BECS.

2. *Flare-to-fenestration diameter ratio* describes the amount of flaring of the BECS relative to the diameter of the fenestration. The minimum and maximum diameters of the BECS at the top of the flare and at the fenestration are calculated from the interpolated circumferences (Figure 8C). The *flare-to-fenestration diameter ratio* is defined as the ratio between the average diameter at the top of the flare and the diameter at the level of the fenestration.

3. *D-ratio* describes the shape of the flare, whereas 1 equals a circle and lower values describe an oval shape and indicate BECS compression. The *D-ratio* is defined as the minor axis divided by the major axis.

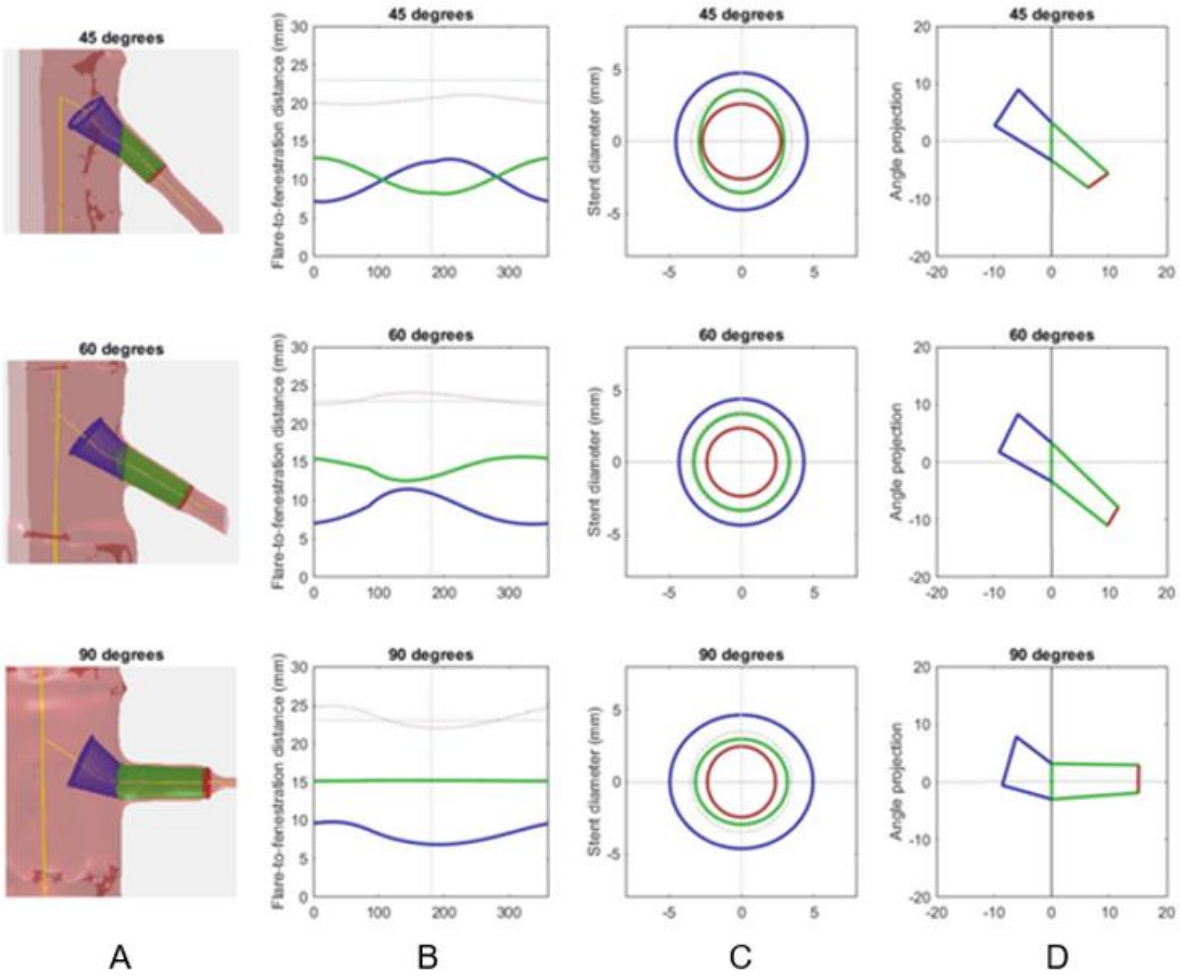

Figure 8: Geometric analysis of the BECSs in three different branch arteries. The blue and green colored surfaces and lines visualize the flared part and the branched part respectively. A) 3D visualization of the BECS. B) Flare-to-fenestration distance. The red dashed line visualizes the calculated length of the BECS and the black dashed line visualizes the known length of the BECS. C) Flare-to-fenestration diameter ratio. The blue, green and red colored lines visualizes the shape of the BECS at the top of the flare, at the fenestration and at the distal end, respectively. D) Side view, the vertical black line represents the wall of the phantom.

Statistics

Data were analyzed using SPSS version 23 statistical software (SPSS Inc., Chicago, Ill). Inter- and intra-observer variabilities were tested for the distances and the diameters of the manual measurements and the geometric analysis by Bland-Altman plots. The gold standard is compared to one set of measurements one observer, Bland-Altman plots of the distances and diameters were visualized. The mean difference of paired measurements was given, and the RC was assessed using the Bland-Altman method. The RC, also known as limits of agreement, is defined as ±1.96 times the SD of the difference of paired observations and describes the 95% confidence interval of the measurement variability.

Results

The phantom model with three BECS was scanned. The manual measurements were performed once by two observers (ED and CR) and the geometric analysis was performed by two observers (RS and CR). The vascular workstation measurements were performed once by RS and twice by CR.

Manual measurements

The manual measurements are summarized in Table 2. The Bland-Altman plots visualize the inter-observer variability for distance and diameter measurements, the mean±SD is 0.43±0.72 mm and 0.10±0.24 mm, respectively (Figure 9 and 10). There was no significant inter-observer difference for the distances (p=0.061) and the diameters (p=0.246). The gold standard defined as the mean of the manual measurements of both observers is calculated in 'Appendix B' and shown in Table 3.

Table 2: Manual measurements presented in mm

Measurement variables	**BECS 1** *45 degrees*		**BECS 2** *60 degrees*		**BECS 3** *90 degrees*	
Observer	*ED*	*CR*	*ED*	*CR*	*ED*	*CR*
L_0	5.6	5.5	6.6	6.5	5.5	6.0
L_{90}	9.0	10.0	8.0	9.0	7.2	8.0
L_{180}	14.6	14.0	13.0	13.0	10.2	10.1
L_{270}	8.9	11.0	9.5	9.8	8.7	9.1
D_{flare1}	8.6	9.1	8.4	8.6	9.2	9.1
D_{flare2}	8.6	8.9	8.2	8.5	9.3	9.0
$D_{fenestration}$	5.0	5.0	4.5	4.5	4.5	4.5

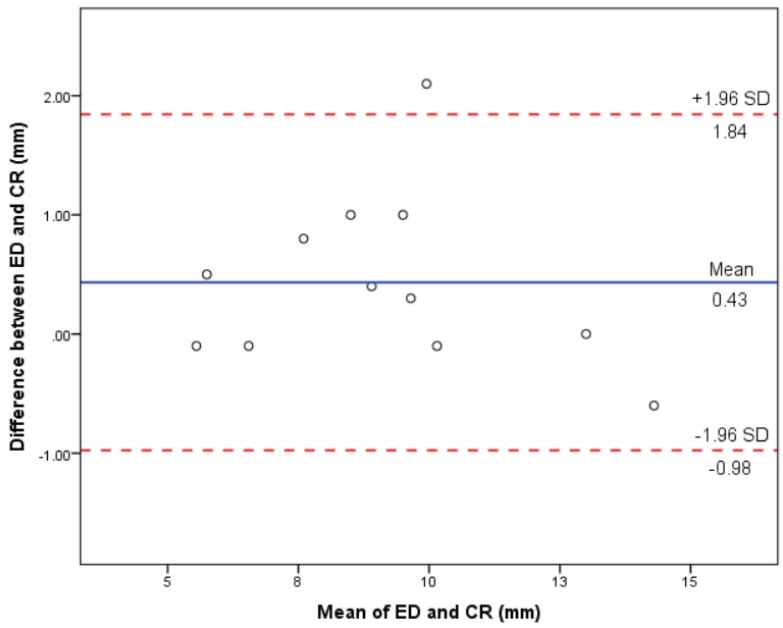

Figure 9: Bland-Altman plot for the inter-observer variability of the distance measurements

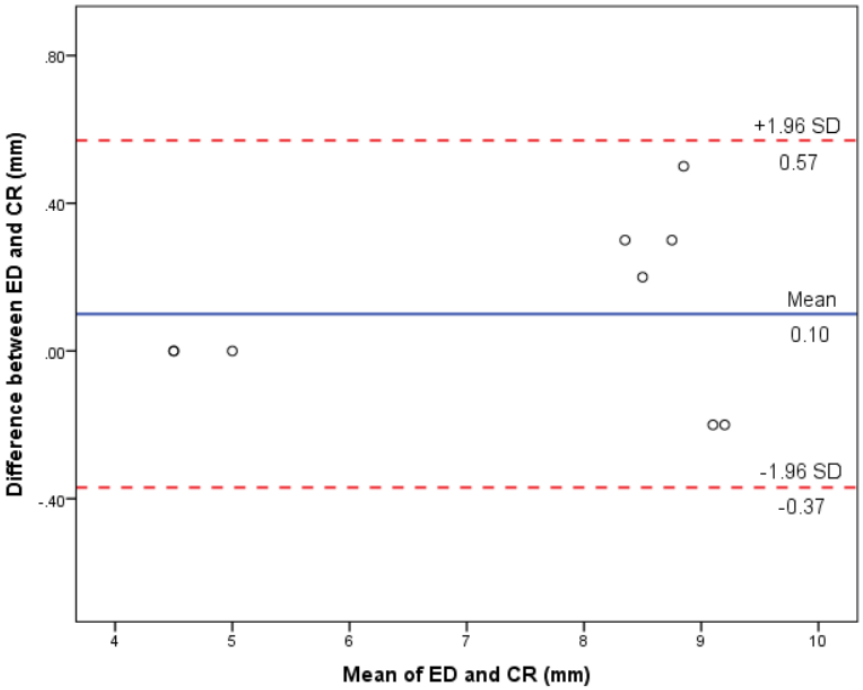

Figure 10: Bland-Altman plot for the inter-observer variability of the diameter measurements

Table 3: Gold standard

Variables	**BECS 1** 45 degrees	**BECS 2** 60 degrees	**BECS 3** 90 degrees
Flare-to-fenestration distance:			
• L_0	5.6	6.6	5.8
• L_{90}	9.5	8.5	7.6
• L_{180}	14.3	13.0	10.2
• L_{270}	10.0	9.7	8.9
Flare-to-fenestration diameter ratio	1.8	1.9	2.0
D-ratio	1.0	1.0	1.0

Geometric analysis

Inter- and intra-observer variability for the distance and diameter measurements of the geometric analysis of the software are visualized in Bland-Altman plots (Figure 11-14). The *flare-to-fenestration distance*, the *flare-to-fenestration diameter ratio* and the *D-ratio* outcomes are shown in Table 4-6.

There was significant difference for the distance measurements (p=0.002) and there was no significant difference for the diameter measurements (p=0.774) of the inter-observer variability. There was no significant difference for the distance (p=0.543) and the diameter measurements (p=0.646) of the inter-observer variability. There was no significant difference for the distance measurements (p=0.676) and there was significant difference for the diameter measurements (p=0.022) for the gold standard compared to one set of the manual measurements of CR.

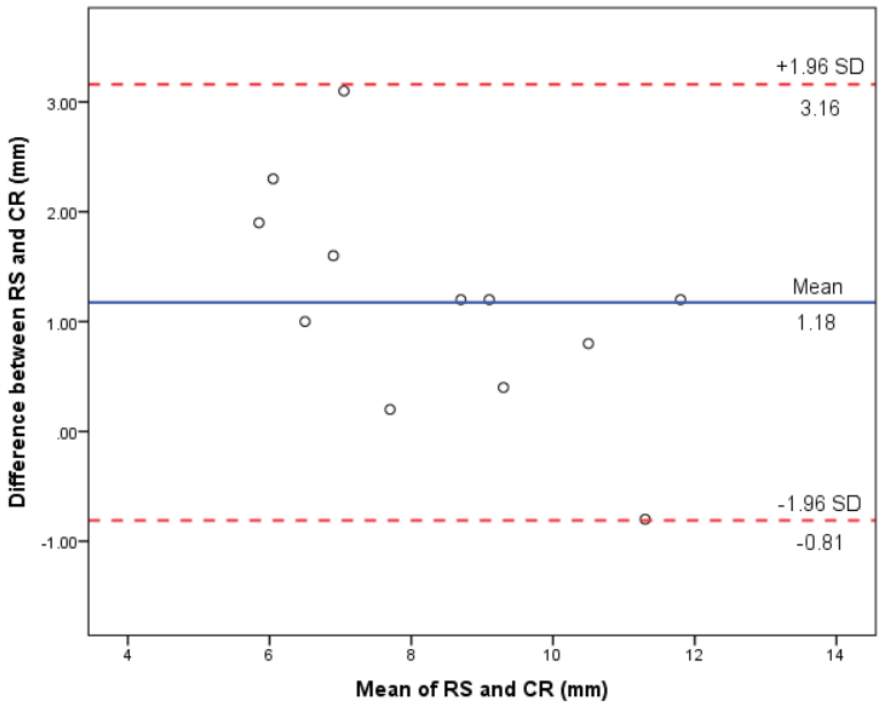

Figure 11: Bland-Altman plot for the inter-observer variability of the distance measurements

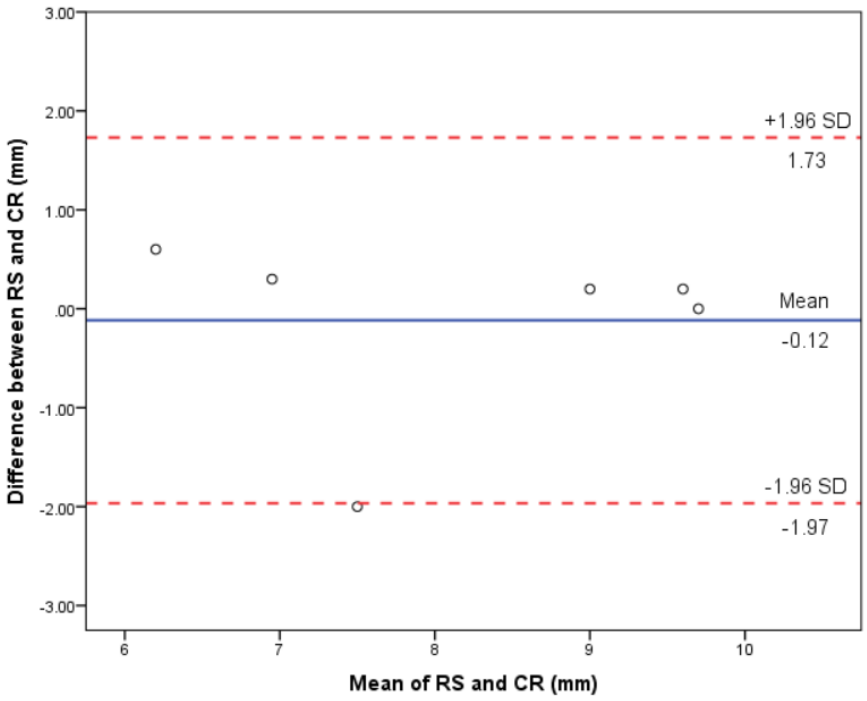

Figure 12: Bland-Altman plot for the inter-observer variability of the diameter measurements

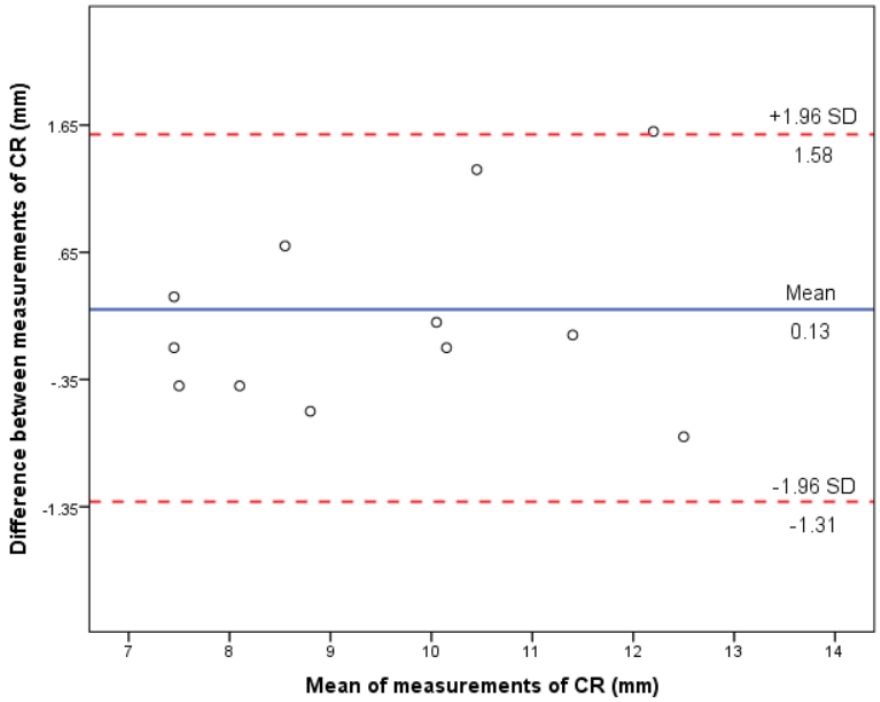

Figure 13: Bland-Altman plot for the intra-observer variability of the distance measurements

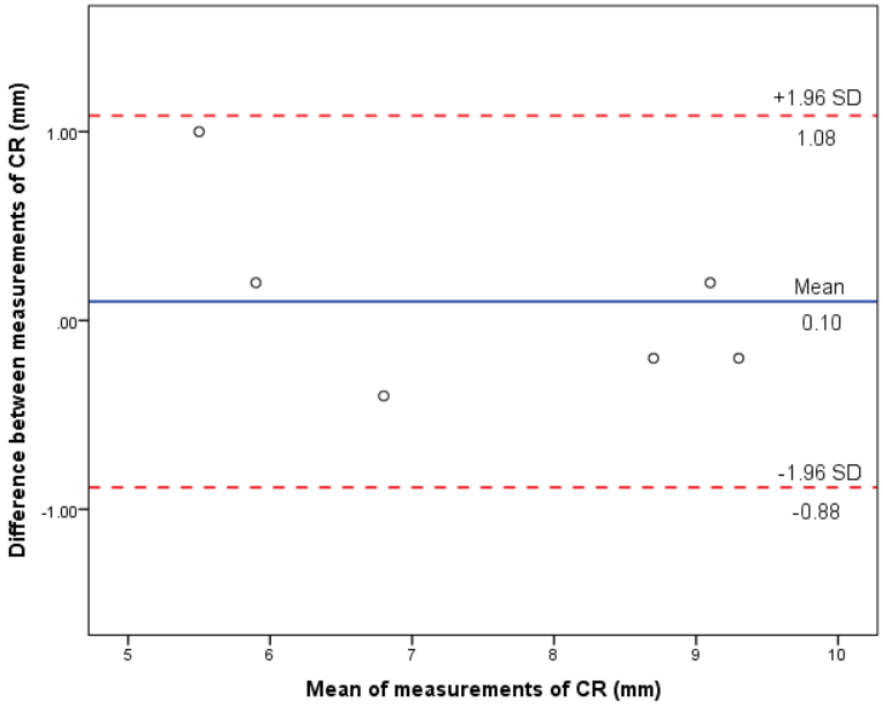

Figure 14: Bland-Altman plot for the intra-observer variability of diameter measurements

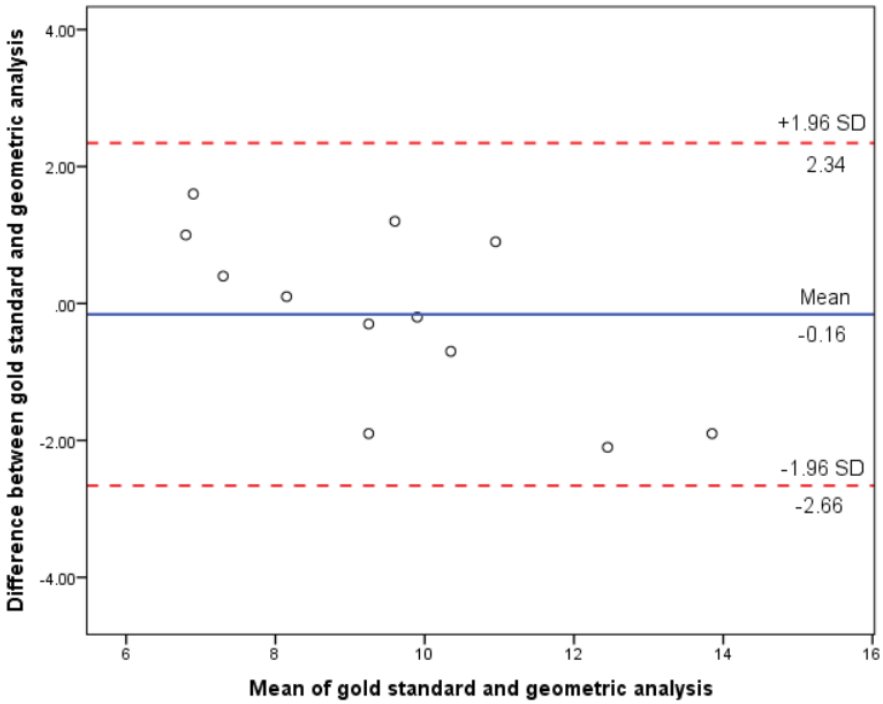

Figure 15: Bland-Altman plot for the gold standard and geometric analysis of the distance measurements

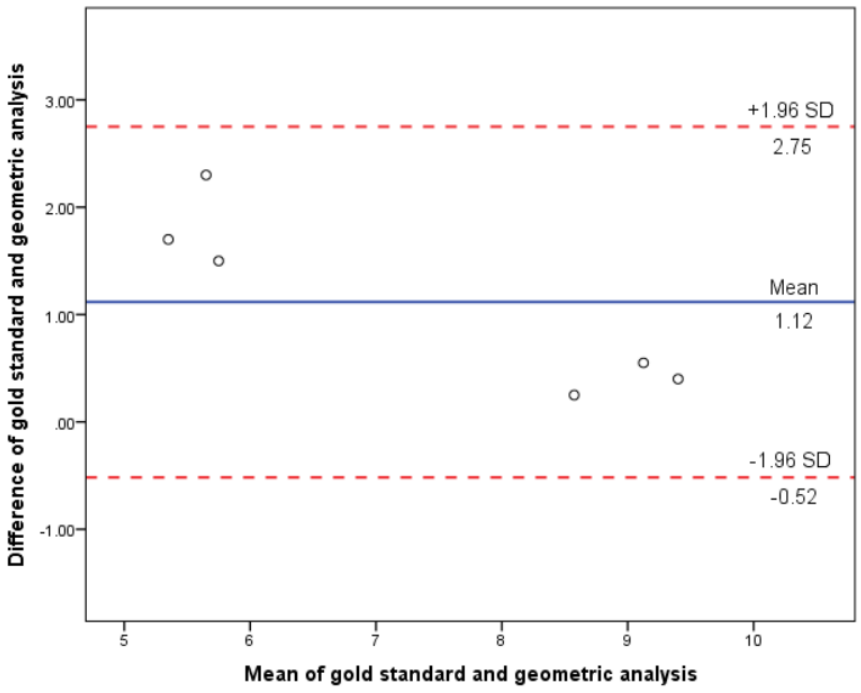

Figure 16: Bland-Altman plot for the gold standard and geometric analysis of the diameter measurements

Table 4: Geometric analysis outcomes of two observers

BeGraft BECS	**BECS 1**		**BECS 2**		**BECS 3**	
	45 degrees		*60 degrees*		*90 degrees*	
Observer	*RS*	*CR*	*RS*	*CR*	*RS*	*CR*
Flare-to-fenestration distance:						
• L_0	4.9	7.2	6.0	7.0	4.9	6.8
• L_{90}	8.0	9.3	8.5	9.7	6.1	7.7
• L_{180}	11.2	12.4	10.1	10.9	9.1	9.5
• L_{270}	11.7	10.9	7.6	7.8	5.5	8.6
Flare-to-fenestration diameter ratio	1.2	1.4	1.2	1.3	1.2	1.5
D-ratio	1.0	1.0	1.0	1.0	1.0	0.9

Table 5: Geometric analysis outcomes of two measurement moments by one observer

BeGraft BECS	**BECS 1**		**BECS 2**		**BECS 3**	
	45 degrees		*60 degrees*		*90 degrees*	
Measurement moment	*1*	*2*	*1*	*2*	*1*	*2*
Flare-to-fenestration distance:						
• L_0	7.2	6.8	7.0	6,9	6,8	7.1
• L_{90}	9.3	10.6	9.7	9.6	7.7	8.4
• L_{180}	12.4	11.6	10.9	10.9	9.5	9.6
• L_{270}	10.9	12.5	7.8	7.4	8.6	8.0
Flare-to-fenestration diameter ratio	1.5	1.3	1.3	1.3	1.6	1.5
D-ratio	1.0	1.0	1.0	0.9	0.9	1.0

Table 6: Parameter outcomes of the gold standard and the geometric analysis

BeGraft BECS	**BECS 1**		**BECS 2**		**BECS 3**	
	45 degrees		*60 degrees*		*90 degrees*	
	Manual	*Software*	*Manual*	*Software*	*Manual*	*Software*
Flare-to-fenestration distance:						
• L_0	5.6	7.2	6.6	7.0	5.8	6.8
• L_{90}	9.5	9.3	8.5	9.7	7.6	7.7
• L_{180}	14.3	12.4	13.0	10.9	10.2	9.5
• L_{270}	10.0	10.9	9.7	7.8	8.9	8.6
Flare-to-fenestration diameter ratio	1.8	1.4	1.9	1.3	2.0	1.5
D-ratio	1.0	0.9	1.0	0.9	1.0	0.9

Discussion

The goal of this study was to provide a standardized and validated post-FEVAR measurement protocol for accurate 3D assessment of the BECS configuration, but that was not realistic with one series of BECS. Validation with one more series of BeGraft BECS and two series of Advanta V12 BECS will be performed as soon as possible. This will provide more insight in the applicability of the software for different BECS and in the changes in BECS configuration over time (when the series were placed differently). The gold standard which was used for the validation was defined as the mean of the manual measurements of both observers. The mean difference of ±0.43 mm and ±0.10 mm for the distance and diameter measurements were acceptable to define the gold standard as the mean of the manual measurements.

The 45°, 60° and 90° branch off arteries of the phantom model represent the celiac trunk, the SMA and the renal arteries, respectively. The flare of BECS 3 differs from the flare of BECS 1, because a larger angle of the flare is needed to position the top of the flare toward the blood flow. Larger differences in the L_{90} and L_{270} manual measurements were expected, because the angle is an additional variable, this is shown in Table 2. In addition, the $D_{fenestration}$ measurements performed with the bore kit represent the smallest diameter and suggest a circle shaped BECS at the level of the fenestration. The geometric analysis showed an ellipse shape for BECS 1 and BECS 3 at the level of the fenestration (Figure 8C). The underestimation of $D_{fenestration}$ in the manual measurements explains the larger *flare-to-fenestration diameter ratio* for the manual measurements compared to the geometric analysis, this is show in Table 6.

The mean and limits of agreement for inter- and intra-observer diameter differences of the geometric analysis were ±0.12 mm and [-1.97, 1.73], and ±0.10 mm and [-0.88, 1.08] respectively. Lu, et al. described an inter-observer variability of ±1.2 mm with limits of agreement [-1.5, +0.9] mm for the maximal diameter of the ascending aorta; whereas intra-observer limits were [-1.2, +1.0] mm and [-0.8, +0.8] mm[34]. This in vitro validation study showed approximately the same intra-observer variability, but larger inter-observer variability. Note, that the measurements of Lu, et al. were performed on a fixed centerline and the analysis of this study were based on too few series of BECS. Both, the inter- and intra-observer variability for the diameter measurements showed acceptable outcomes. The limiting factors were the slice thickness (0.75 mm) and the BECS' CLL with an accuracy of 1 mm in the vascular workstation.

The gold standard was compared to one set of measurements of CR and showed reliable mean differences for the distance and diameter measurements: ±0.16 mm and ±1.12 mm, respectively. The limits of agreement for the distances [-2.66, 2.34] mm and diameters [-0.52, 2.75] were relatively large. The diameter differences were significant: $D_{fenestration}$ showed larger differences than D_{flare}. More measurements need to be performed to be able to make conclusion about the quantification. The geometric analysis provides a good visualization which can support the vascular surgeon but cannot be used as the "decision maker" in the clinical practice. An accuracy of approximately 1 mm is needed, but that is not feasible with the currently available techniques.

Conclusion

The geometric analysis performed by dedicated software functions with an acceptable inter- and intra-observer variability with the current limitations, but more measurements must be performed. The accuracy of the geometric analysis is limited by the slice thickness and the centerline in the vascular workstation. The visualization can support the clinical practice but a precise quantification is not reachable with the currently available techniques.

Chapter 4 – Future perspectives

Vascular workstation and software

Several extensions of the vascular workstation 3Mensio and the software may facilitate clinical implementation. In the vascular workstation this may include keyboard shortcuts for the placement of coordinate markers, the option to give them a name for a clear overview and to group them. Grouping helps the software to distinguish the coordinate markers at the top of the flare, the fenestration and the distal end of the BECS.

In the software, implementation of the calculation of the angle between the FSG and the BECS at 0° reference point result in a more complete geometric analysis. Kandail, et al. concluded that smaller dilation angles and a shorter *flare-to-fenestration distance* are likely to reduce the risk of thrombosis in flared geometries[35]. In addition, a higher angle of curvature leads to higher hemodynamic forces that result in a higher rate of thrombosis according to Fidalgo-Domingos, et al. [36].

BECS design and FEVAR procedure

The BECS design influences the way of flaring. The Advanta V12 BECS is produced as one part. A BECS consisting of two parts: a flared part and a branched part with their own characteristics could optimize the flare. Ideally, the *flare-to-fenestration distance* is zero (Figure 1). This reduces the hemodynamic forces which act on the connection and this makes it possible to add an extra fixation to the flare. In the future, it could be possible to produce a FSG with integrated and fixated BECS.

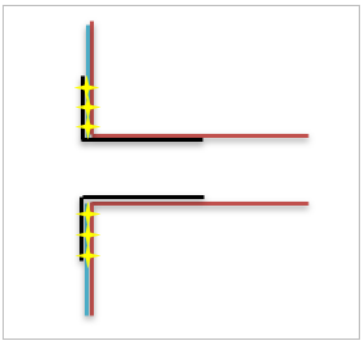

Figure 1: Schematic side view of the flare of two-part BECS design. The red lines visualize the aorta, the blue lines visualize the FSG, the black lines visualize the BECS and additional anchoring is yellow colored.

Early clinical outcomes and geometric analysis based on the first pre-operative CTA scan could result in a patient-specific follow-up. In case of no complications, this should result in less imaging moments and thus less nephrotoxic contrast and exposure to ionizing radiation for the patient[37]. In case of complications, this should result in complication detection before urgent re-intervention is needed.

The outcomes of the FEVAR procedure are influenced by the performance of the surgical team[38]. The team have a learning curve and this curve could be improved due to training in a simulator with virtual reality or by training with 3D models of an AAA before the FEVAR procedure.

Validation study

After the validation study is completed with one series of BeGraft BECS and two series Advanta V12 BECS the next step consists of retrospective analysis of patients' CTA scans. Firstly, the first post-FEVAR

and the latest CTA scan of patients with an uncomplicated follow-up should be analyzed to detect (standard) changes in the BECS and FSG. Secondly, all post-FEVAR CTA scans up to and including the BECS complication should be analyzed to detect changes over time before the complication. This will provide insight in the possibility to discover complications before urgent re-intervention is needed.

The geometric analysis provides information about the stent patency based on distances and diameters. Stent fractures were not involved in this analysis, but patency rates were affected by stent fractures[15]. Quantification and visualization of FSG motion in ECG-gated CT has been validated and tested in vivo by Koenrades, et al. [39]. Geometric analysis of ECG-gated CT scans could reveal stent fractures. An update of the software is needed before further investigation of in situ motion of BECS and their interaction with target arteries is possible.

Bibliography

1. Johnston, K.W., et al., *Suggested standards for reporting on arterial aneurysms. Subcommittee on Reporting Standards for Arterial Aneurysms, Ad Hoc Committee on Reporting Standards, Society for Vascular Surgery and North American Chapter, International Society for Cardiovascular Surgery.* J Vasc Surg, 1991. **13**(3): p. 452-8.
2. Sakalihasan, N., et al., *Modifications of the extracellular matrix of aneurysmal abdominal aortas as a function of their size.* Eur J Vasc Surg, 1993. **7**(6): p. 633-7.
3. Cornuz, J., et al., *Risk factors for asymptomatic abdominal aortic aneurysm: systematic review and meta-analysis of population-based screening studies.* Eur J Public Health, 2004. **14**(4): p. 343-9.
4. Chaikof, E.L., et al., *The Society for Vascular Surgery practice guidelines on the care of patients with an abdominal aortic aneurysm.* J Vasc Surg, 2018. **67**(1): p. 2-77.e2.
5. Reimerink, J.J., et al., *Systematic review and meta-analysis of population-based mortality from ruptured abdominal aortic aneurysm.* Br J Surg, 2013. **100**(11): p. 1405-13.
6. Moll, F.L., et al., *Management of abdominal aortic aneurysms clinical practice guidelines of the European society for vascular surgery.* Eur J Vasc Endovasc Surg, 2011. **41 Suppl 1**: p. S1-S58.
7. Furuya, T., *[Open repair for pararenal abdominal aortic aneurysm: the strategy and pitfalls for safe surgery].* Nihon Geka Gakkai Zasshi, 2011. **112**(1): p. 17-21.
8. Febbo, B., *Aortic Aneurysm: Clinical Highlights/Updates.* http://www.foamem.com/2015/03/25/abdominal-aortic-aneurysm-clinical-highlightsupdates/, 2015.
9. Varkevisser, R.R.B., et al., *Fenestrated endovascular aneurysm repair is associated with lower perioperative morbidity and mortality compared with open repair for complex abdominal aortic aneurysms.* J Vasc Surg, 2019. **69**(6): p. 1670-1678.
10. Belvroy, V.M., et al., *Identifying and addressing the limitations of EVAR technology.* Expert Rev Med Devices, 2018. **15**(8): p. 541-554.
11. Wanhainen, A., et al., *European Society for Vascular Surgery (ESVS) 2019 Clinical Practice Guidelines on the Management of Abdominal Aorto-iliac Artery Aneurysms.* https://www.ejves.com/article/S1078-5884(18)30698-1/fulltext, 2019.
12. Hu, Z., et al., *Experience With Fenestrated Endovascular Repair of Juxtarenal Abdominal Aortic Aneurysms at a Single Center.* Medicine (Baltimore), 2016. **95**(10): p. e2683.
13. Timaran, C.H., et al., *The sequential catheterization amid progressive endograft deployment technique for fenestrated endovascular aortic aneurysm repair.* J Vasc Surg, 2017. **66**(1): p. 311-315.
14. Mwipatayi, B.P., et al., *Durability of the balloon-expandable covered versus bare-metal stents in the Covered versus Balloon Expandable Stent Trial (COBEST) for the treatment of aortoiliac occlusive disease.* J Vasc Surg, 2016. **64**(1): p. 83-94.e1.
15. Grimme, F.A., et al., *Visceral stent patency in fenestrated stent grafting for abdominal aortic aneurysm repair.* J Vasc Surg, 2014. **59**(2): p. 298-306.
16. Hu, Z., et al., *Experience With Fenestrated Endovascular Repair of Juxtarenal Abdominal Aortic Aneurysms at a Single Center.* Medicine, 2016. **95**: p. e2683.
17. Sayed, T., et al., *Jotec E-Ventus BX Stent Graft Deployment in the FEVAR and Iliac Branch Device: Single Centre Experience.* Ann Vasc Dis, 2019. **12**(2): p. 171-175.
18. Yapa, S.M. and K. Sieunarine, *Late renal artery stent fracture with pseudoaneurysm after fenestrated endovascular abdominal aortic aneurysm repair.* J Vasc Surg Cases Innov Tech, 2019. **5**(2): p. 149-151.
19. Schuurman, J.P., et al., *Renal artery pseudoaneurysm caused by a complete stent fracture: a case report.* J Vasc Surg, 2009. **49**(1): p. 214-6.

20. Ambler, G., *Early results of fenestrated endovascular repair of juxtarenal aortic aneurysms in the United Kingdom.* Circulation, 2012. **125**(22): p. 2707-15.
21. Roy, I.N., et al., *Long-term follow-up of fenestrated endovascular repair for juxtarenal aortic aneurysm.* Br J Surg, 2017. **104**(8): p. 1020-1027.
22. O'Callaghan, A., et al., *Type Ia endoleaks after fenestrated and branched endografts may lead to component instability and increased aortic mortality.* J Vasc Surg, 2015. **61**(4): p. 908-14.
23. Mastracci, T.M., et al., *Durability of branches in branched and fenestrated endografts.* J Vasc Surg, 2013. **57**(4): p. 926-33; discussion 933.
24. Pandey, N. and H.I. Litt, *Surveillance Imaging Following Endovascular Aneurysm Repair.* Semin Intervent Radiol, 2015. **32**(3): p. 239-48.
25. Mazzei, M.A., et al., *Follow-up of endovascular aortic aneurysm repair: Preliminary validation of digital tomosynthesis and contrast enhanced ultrasound in detection of medium- to long-term complications.* World J Radiol, 2016. **8**(5): p. 530-6.
26. Cao, P., et al., *Endoleak after endovascular aortic repair: classification, diagnosis and management following endovascular thoracic and abdominal aortic repair.* J Cardiovasc Surg (Torino), 2010. **51**(1): p. 53-69.
27. Shivananda, A., D'Souza, D., et al., *Endoleak.* https://radiopaedia.org/articles/endoleak, 2017.
28. Jain, A., et al., *VESS10. Natural History of Target Vessel Endoleaks After Fenestrated-Branched Endovascular Aortic Repair.* Journal of Vascular Surgery, 2018. **67**: p. e53-e54.
29. England, A., M. Garcia-Finana, and R.G. McWilliams, *Multicenter retrospective investigation into migration of fenestrated aortic stent grafts.* J Vasc Surg, 2015. **62**(4): p. 884-92.
30. Robertson, S.W., et al., *Right renal artery in vivo stent fracture.* J Vasc Interv Radiol, 2008. **19**(3): p. 439-42.
31. Suh, G.Y., et al., *Three-Dimensional Modeling Analysis of Visceral Arteries and Kidneys during Respiration.* Ann Vasc Surg, 2016. **34**: p. 250-60.
32. de Niet, A., et al., *Geometric changes over time in bridging stents after branched and fenestrated endovascular repair for thoracoabdominal aneurysm.* J Vasc Surg, 2019. **70**(3): p. 702-709.
33. Overeem, S., et al., *Validation of a Novel Methodology to Evaluate Changes in the Flare Geometry of Renovisceral Bridging Stent-Grafts After Fenestrated Endovascular Aneurysm Repair.* J Endovasc Ther, 2020: p. 1526602820915932.
34. Lu, T.L., et al., *Variability of ascending aorta diameter measurements as assessed with electrocardiography-gated multidetector computerized tomography and computer assisted diagnosis software.* Interact Cardiovasc Thorac Surg, 2010. **10**(2): p. 217-21.
35. Kandail, H., M. Hamady, and X.Y. Xu, *Effect of a Flared Renal Stent on the Performance of Fenestrated Stent-Grafts at Rest and Exercise Conditions.* J Endovasc Ther, 2016. **23**(5): p. 809-20.
36. Fidalgo-Domingos, L., et al., *Geometric and hemodynamic analysis of fenestrated and multibranched aortic endografts.* J Vasc Surg, 2020.
37. Horinouchi, H., et al., *CT angiography with 15 mL contrast material injection on time-resolved imaging for endovascular abdominal aortic aneurysm repair.* Eur J Radiol, 2020. **126**: p. 108861.
38. Baron, V. and R. Guevara, *Three-dimensional printing-guided fenestrated endovascular aortic aneurysm repair using open source software and physician-modified devices.* J Vasc Surg Cases Innov Tech, 2019. **5**(4): p. 566-571.
39. Koenrades, M.A., et al., *Quantitative Stent Graft Motion in ECG Gated CT by Image Registration and Segmentation: In Vitro Validation and Preliminary Clinical Results.* European Journal of Vascular and Endovascular Surgery, 2019. **58**(5): p. 746-755.

Appendices

Appendix A

Additional analysis of Chapter 2

The freedom from re-intervention per patient with different number of fenestrations is presented as a Kaplan-Meier curve (Figure 1). Patients who underwent 2-FEVAR showed less re-interventions than patients who underwent 3-FEVAR at 6 years follow-up. There are two plausible explanations for this; 1) there are more fenestrations needed in case of a more complex aneurysm and this indicates a sicker aorta, 2) more BECS in situ increases the risk of complications and thus re-intervention. In contrast, to less fenestrations can result in decreased seal of the FSG and causes type 1a endoleak. 2- and 3-FEVAR re-interventions rates cannot be compared to 1- and 4-FEVAR, due to the differences in number at risk. In addition, there were to less 1- and 4-FEVAR cases in this cohort to draw conclusion about freedom from re-intervention.

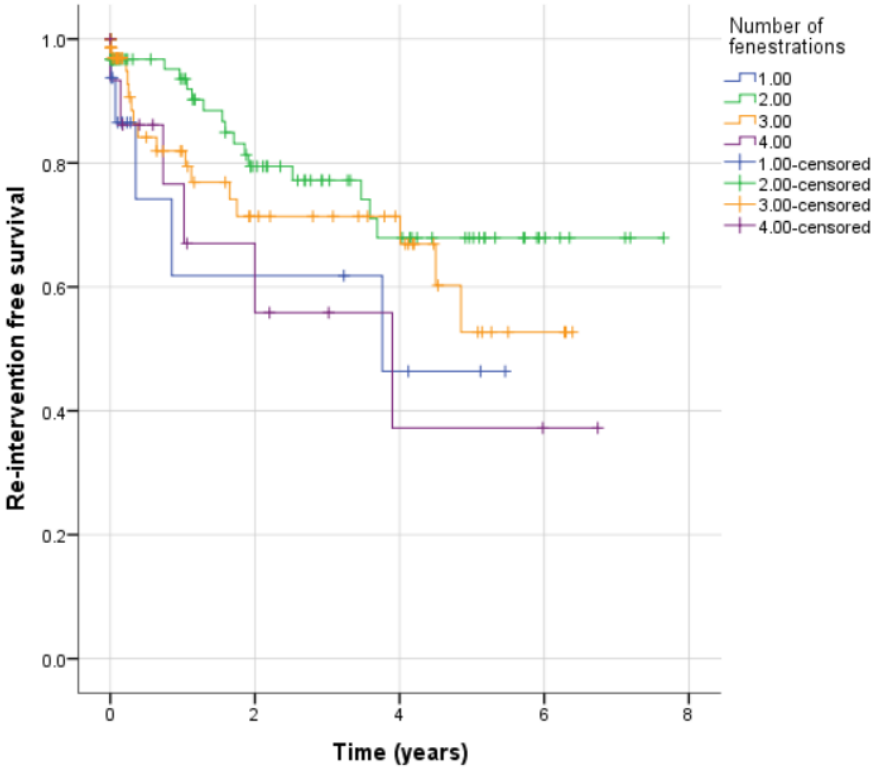

Number at risk				
1-FEVAR	16	5	3	0
2-FEVAR	92	40	22	6
3-FEVAR	72	24	16	3
4-FEVAR	15	6	2	1

Figure 1: Kaplan-Meier curve for re-intervention-free survival visualized per number of fenestrations per patient

Appendix B

Calculated variables of Chapter 3

Table 1: Parameter outcomes based on manual measurements of two observers

Measurement variables	**BECS 1** *45 degrees*		**BECS 2** *60 degrees*		**BECS 3** *90 degrees*	
Observer	*ED*	*CR*	*ED*	*CR*	*ED*	*CR*
D_{flare1}	8.6	9.1	8.4	8.6	9.2	9.1
D_{flare2}	8.6	8.9	8.2	8.5	9.3	9.0
$D_{fenestration}$	5.0	5.0	4.5	4.5	4.5	4.5
Calculated variables						
$D_{flare\text{-}average}$	8.60	9.00	8.30	8.55	9.25	9.05
Flare-to-fenestration diameter ratio	1.72	1.80	1.84	1.90	2.05	2.01
D-ratio	1.00	0.98	0.98	0.99	0.99	0.99

Table 2: Parameter outcomes based on the geometric analysis of two observers

BeGraft BECS	**BECS 1** *45 degrees*		**BECS 2** *60 degrees*		**BECS 3** *90 degrees*	
Observer	*RS*	*CR*	*RS*	*CR*	*RS*	*CR*
D_{flare1}	9.0	9.2	8.4	8.6	9.2	9.2
D_{flare2}	9.0	9.6	8.6	8.8	9.5	10.0
$D_{fenestration\text{-}min}$	5.4	6.0	6.3	6.6	8.0	6.0
$D_{fenestration\text{-}max}$	9.6	7.0	7.4	7.0	8.0	6.4
Calculated variables						
$D_{flare\text{-}average}$	9.0	9.4	8.5	8.7	9.4	9.6
$D_{fenestration\text{-}average}$	7.5	6.5	6.9	6.8	8.0	6.2
Flare-to-fenestration diameter ratio	1.2	1.4	1.2	1.3	1.2	1.5
D-ratio	1.0	1.0	1.0	1.0	1.0	0.9

Table 3: Parameter outcomes based on the geometric analysis of two measurement moments performed by CR

BeGraft BECS	**BECS 1** *45 degrees*		**BECS 2** *60 degrees*		**BECS 3** *90 degrees*	
Measurement moment	*1*	*2*	*1*	*2*	*1*	*2*
D_{flare1}	9.2	9.0	8.6	8.8	9.2	9.4
D_{flare2}	9.6	9.2	8.8	9.4	10.0	9.4
$D_{fenestration\text{-}min}$	6.0	5.0	6.6	7.0	6.0	5.8
$D_{fenestration\text{-}max}$	7.0	8.6	7.0	7.6	6.4	6.4
Calculated variables						
$D_{flare\text{-}average}$	9.4	9.1	8.7	9.1	9.6	9.4
$D_{fenestration\text{-}average}$	6.5	6.8	6.8	7.3	6.2	6.1
Flare-to-fenestration diameter ratio	1.5	1.3	1.3	1.3	1.6	1.5
D-ratio	1.0	1.0	1.0	0.9	0.9	1.0

Table 4: Parameter outcomes for the gold standard and the geometric analysis based on the first measurements of CR

Measurement variables	**BECS 1** *45 degrees*		**BECS 2** *60 degrees*		**BECS 3** *90 degrees*	
	Manual	*Software*	*Manual*	*Software*	*Manual*	*Software*
D_{flare1}	8.9	9.2	8.5	8.6	9.2	9.2
D_{flare2}	8.8	9.6	8.4	8.8	9.2	10.0
$D_{fenestration\text{-}min}$	5.0	6.0	4.5	6.6	4.5	6.0
$D_{fenestration\text{-}max}$	x	7.0	x	7.0	x	6.4
Calculated variables						
$D_{flare\text{-}average}$	8.9	9.4	8.5	8.7	9.2	9.6
$D_{fenestration\text{-}average}$	5.0	6.5	4.5	6.8	4.5	6.2
Flare-to-fenestration diameter ratio	1.8	1.4	1.9	1.3	2.0	1.5
D-ratio	1.0	0.9	1.0	0.9	1.0	0.9